Journal of Building Engineering 80 (2023) 108037

Contents lists available at ScienceDirect

Journal of Building Engineering

journal homepage: www.elsevier.com/locate/jobe

Full length article

Ballistic limit and damage assessment of hybrid fibre-reinforced cementitious thin composite plates under impact loading

Cesare Signorini [a,*], Franz Bracklow [b], Marcus Hering [b,c], Marko Butler [a], Lena Leicht [b], Thomas Schubert [b], Mirza A.B. Beigh [a], Birgit Beckmann [b], Manfred Curbach [b], Viktor Mechtcherine [a]

[a] Institute of Construction Materials, TU Dresden, 01187 Dresden, Germany
[b] Institute of Concrete Structures, TU Dresden, 01062 Dresden, Germany
[c] Bundesanstalt für Materialforschung und –prüfung (BAM), 12205 Berlin, Germany

ARTICLE INFO

Keywords:
Impact loading
Cement-based composites
SHCC
TRC
Sustainable binders

ABSTRACT

Impact resistance of reinforced concrete (RC) structures can be significantly improved by strengthening RC members with thin composite layers featuring high damage tolerance. Indeed, to limit the well-known vulnerability of cement-based materials against impact loading, the synergistic effects of short fibres and continuous textile meshes as hybrid reinforcement has been proved to be highly beneficial. This paper addresses the characterisation of novel cement-based hybrid composites through accelerated drop-weight impact tests conducted on rectangular plates at different impact energies. Two distinct matrices are assessed, with particular interest in a newly developed limestone calcined clay cement (LC^3)-based formulation. Important parameters quantifying energy dissipation capability, load bearing capacity and damage are cross-checked to compute the ballistic limit and estimate the safety-relevant characteristics of the different composites at hand. Although textiles alone can improve the damage tolerance of fine concrete to some extent, the crack-bridging attitude of short, well-dispersed fibres in hybrid composites imparts a certain ductility to the cement-based matrices, allowing a greater portion of the textile to be activated and significantly reducing the amount of matrix spalling under impact.

1. Introduction

The popularity of concrete as structural material is well established nowadays. In fact, the majority of civil, industrial and military structures and infrastructure built in the last century have been made of reinforced concrete (RC). When combined with steel rebar, concrete can effectively withstand common loading conditions, and represents the most viable solution with respect to cost-to-performance ratio. To maintain the structural functionality of RC members over time in terms of load-bearing capacity and ductility, externally bonded reinforcements made from composite materials including short fibres and/or multifilament textiles have been widely recognised as efficient solutions [1–3]. In particular, ductility and dissipation capability are essential criteria driving the design approach to successfully withstand sudden extreme loading conditions, brought into play e.g. by climate change and military implications [4]. Traditionally, fabric (or fibre) reinforced polymer (FRP) composites have been developed and have shown considerable potential for retrofitting structural elements under dynamic loading regimes, such as blast and explosions [5,6]. A detailed case history of FRP applications in this field is documented in the comprehensive review by Pham and Hao [7]. More

* Corresponding author.
E-mail address: cesare.signorini@tu-dresden.de (C. Signorini).

https://doi.org/10.1016/j.jobe.2023.108037
Received 31 July 2023; Received in revised form 17 October 2023; Accepted 27 October 2023
Available online 30 October 2023

recently, externally-bonded retrofitting materials and systems based on mineral matrices have gained increasing interest [8], in an attempt to overcome the limitations of polymer matrices, such as their poor thermal stability and inapplicability in humid environments [9–11].

Among the varieties of mineral-bonded fibre-reinforced materials, commonly referred to as fibre-reinforced concrete (FRC), the beneficial effects of strain-hardening cement-based composites (SHCC) in enhancing the damage tolerance of RC structures have been highlighted [12,13]. Indeed, the tensile response of SHCC is quasi-ductile, holistically resembling the typical behaviour of metals [14]. The propensity of SHCC to undertake a finely distributed cracking pattern under tension is crucial for inducing a pronounced strain hardening behaviour after the formation of the first crack. This peculiar behaviour allows for the dissipation of a considerable amount of mechanical energy, outperforming by far other types of FRC [15], and fostering good protection against environmental agents, thus extending the durability of vulnerable structures such as chimneys, tall buildings, off-shore structures, wind turbines etc. [16]. In addition to the promising durability benefits, SHCC protective layers exhibit exceptional response to impact loading, as demonstrated by various material scale studies, using Split-Hopkinson bar [17–21], Charpy-like hammer [22] and drop-weight tests [23,24], and validated by advanced numerical approaches [25].

On a larger scale, Elnagar et al. [12] tested RC slabs (500 mm sided) in a gravitational drop-weight facility, dropping the impactor from different heights. The RC slabs were reinforced with thin layers of SHCC, and it was observed that different mechanical treatments of the substrate resulted in different mechanical performance. In particular, for slabs strengthened with SHCC on the tension side, roughening the surface by grinding the substrate together with the application of an epoxy adhesive layer yielded the most improved impact performance. Hering et al. [26] benchmarked the impact performance and dissipation capacity of thin fine-grained concrete slabs. The experiments were conducted in an 11-meter drop-tower facility, which is ideal for characterising the structural performance of concrete elements. The data reported therein served as a reference for the current study.

On the structural level, Figueiredo et al. [13] recently published a study discussing the modal analysis of damaged beams reinforced on the lateral faces with thin SHCC layers and subjected to impact, revealing an outstanding enhancement in the shear performance brought about by the strengthening system.

Structural strengthening can also be achieved by using continuous fibre bundles, in the form of textiles as reinforcing elements of fine-grained cement-based matrices. Batarlar et al. [27] have shown how textile-reinforced concrete (TRC) reinforcement applied on concrete slabs can successfully prevent concrete scabbing, envisaging a significant increase in impact safety. In this case, the membrane effect exerted by the textiles plays an important role, especially in achieving good resilience under repeated impact loading. Hering and Curbach [28] pointed out the crucial role of textile design in terms of choice of fibres. In fact, compared to glass fibres, the exceptional strength and Young's modulus of carbon fibres resulted in better performance. Combining the properties of SHCC and TRC, another family of mineral-bonded hybrid composites can be regarded as textile-reinforced-SHCC (TR-SHCC) [29,30].

This paper deals with the characterisation of a newly developed SHCC based on limestone calcined clay cement (LC^3) matrix, specifically designed to act as a thin strengthening layer for RC members, with and without the addition of 2-ply crossed carbon textiles. The results are compared with a reference composite as a benchmark, and with previous results obtained in the framework of the Research Training Group (RTG) 2250 at the TU Dresden. Critical data processing allows for an objective inference of some important material parameters which are essential for the proper design of impact strengthening layers, e.g. energy dissipation capability, strength and penetration velocity. The enrichment of the database is also pivotal to undertaking robust sustainability analysis and optimised material design strategies, as novel matrices are constantly being developed.

Concept of ballistic limit

When dealing with either gravitational or accelerated drop-weight test set-ups, three possible damage scenarios can be identified, depending on the striking velocity of the impactor ($v_1 > 0$), as schematically shown in Fig. 1a.

Firstly, in case of low impact velocities, *rebound* may occur, resulting in a residual velocity of the impactor in the opposite direction ($v_2 < 0$). Secondly, at higher impact velocities, complete *perforation* occurs, i.e. the impactor passes through the plate, and the residual velocity remains in the direction of impact ($v_2 > 0$). According to the study carried out by Liu et al. [31] on polymer composites, and later validated for glass TRC elements by Wastiels et al. [32], in both the rebound (green dashed line) and perforation (red dash-dotted line) domains, the energy dissipation (ΔE_{kin}) is lower than the input energy ($E_{kin,1}$), as the impactor still embodies kinetic energy after the collision (see the explanatory chart of Fig. 1b). Between the rebound and perforation domains, a limit configuration is attained when the projectile remains embedded into the plate ($v_2 = 0$) [33], which is regarded as the *penetration domain* (orange solid segment). Within the penetration domain, the impact energy is completely absorbed by the target, laying on the so-called *equal-energy* domain, represented by the bisector of the ΔE_{kin}–$E_{kin,1}$ diagram. The velocities at which penetration and perforation first occur can be defined as v_{pen} and v_{perf}, respectively, representing the lower and the upper boundaries of the penetration domain. A similar damage classification has also been proposed by Vossoughi et al. [34] for structural concrete panels reinforced with externally bonded protective mat layers. Depending on the ratio between the target thickness (H) and the projectile diameter (d), the amplitude of the penetration domain can be extremely variable. As a general tendency, the coupling of thick targets and small projectiles, i.e. $H/d \gg 1$, results in a wide penetration range [35].

On the other hand, when the H/d ratio is significantly lower than 1, which is usually the case for thin slabs, the penetration domain tends to collapse into a point, making the distinction between penetration and perforation velocity insignificant. In the latter case, the concept of *penetration limit*, or *ballistic limit* (subscript "*bl*"), intended as the minimum impact velocity (and, similarly, kinetic energy) required to achieve complete perforation of the plate [36], can be defined as $v_{pen} = v_{perf} =: v_{bl}$ ($E_{kin,pen} = E_{kin,perf} =: E_{kin,bl}$). The concept of ballistic limit has been extended also to thick plates on a structural scale, however, the objective assessment of a clear

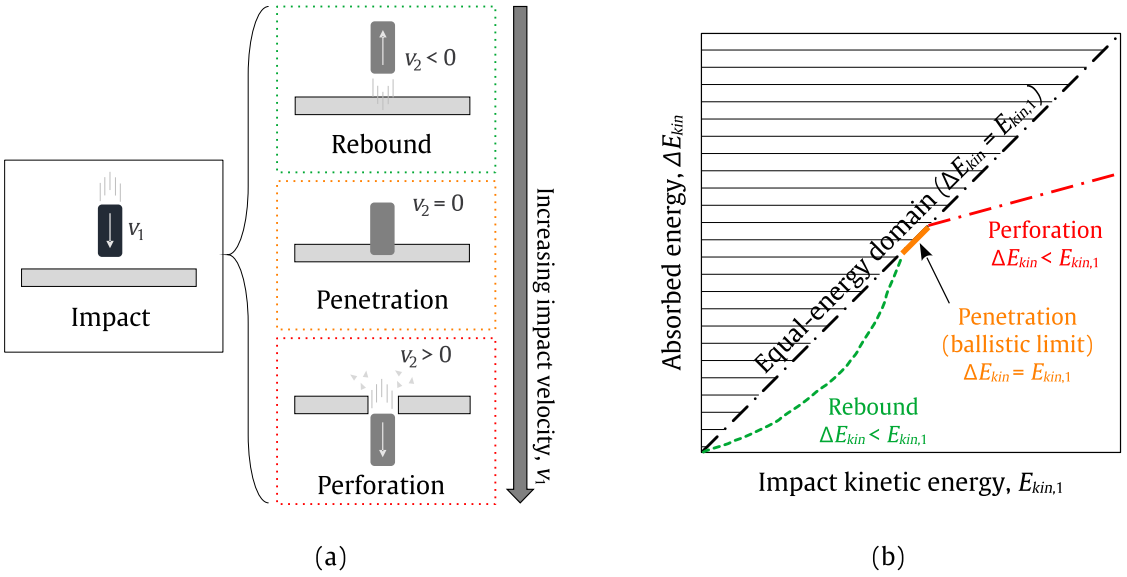

Fig. 1. (a) Different damage scenarios of impact tests on slabs. (b) Qualitative trend of dissipation capability (ΔE_{kin}) vs impact input energy $E_{kin,1}$ of slabs by failure mode.
Source: adapted from Liu et al. [31]

threshold is not trivial, and conventional criteria need to be proposed. In their study about thick slabs, Tahenti et al. [37] identified lower and upper boundaries of the penetration domain, thereby defined by v_0 and v_{100}, namely the velocities at which the probability of perforation is 0% and 100%, respectively. The value of the equivalent velocity v_{50}, predicting a 50% probability of perforation, was therein conventionally proposed as the ballistic limit. Other existing studies at the structural level have proposed experimental [38] and semi-empirical approaches [39,40] to determine the ballistic limit of thick plates struck by small projectiles. Few studies have focused on the concept of ballistic limit for thinner members. Peng et al. [41] proposed a unified penetration modelling framework for various types of ultra-high performance steel fibre reinforced concrete (UHPSFRC) targets with a thickness more than 5 times smaller than the projectile diameter. This approach is based on the hourglass shape of the fracture body, with a front and rear conical crater. Conversely, Hering et al. [42] recently proposed a practical analytical method to identify the ballistic limit of thin plates, based on impact experiments mainly conducted in the perforation domain. This threshold can be obtained analytically by linear fitting of experimental data measured for perforation tests only. In the same way, Wastiels et al. [32] proposed a quantitative characterisation of glass fibre TRC elements under drop-weight impact loading, by assessing the influence of slab thickness and projectile diameter. Therein, the energy profiling method, first developed by Liu et al. [31] for polymer composites, was adapted to identify the penetration limit in cementitious materials, demonstrating its wider validity. Both studies conducted experiments in the rebound domain, and the results are consistent with the assumptions made by Hering et al. [42], and hereafter considered in this study.

2. Materials and methods

2.1. Raw materials

2.1.1. Cement-based fine concrete mixtures

Two formulations or high-strength fine-grained strengthening mortars are adopted as the basis for strain-hardening cement-based composites (SHCC) to be characterised under impact loading. The two compositions consider two different blended binders, including ordinary Portland cement (OPC) and supplementary cementitious materials (SCMs) in a consistent 1:1 weight ratio. More specifically, a newly developed SHCC mix designed according to the LC^3 concept [43] is compared with a reference mix containing fly ash as SCM (FA), which is considered as a benchmark. The fly ash used accounts for an amorphous phase of 75.5%, a BET specific surface area of 1.43 m^2/g and an average particle size D_{50} of 14.80 μm. The full mineralogical composition of the fly ash is reported by Yazdi et al. [44, Table 2]. The compositions in terms of mass per unit volume are given in Table 1, and their rheological properties have been optimised for automated application technologies, e.g., shotcrete and extrusion [45].

Cement (type I) with a compressive strength of 52.5 MPa is used for both matrices. The calcined clay adopted in the present study is retrieved from a low-grade raw clay variety with a kaolinite content of 25%, which has been shown to trigger high pozzolanic reaction in cementitious pastes, yielding 55.7% of amorphous content after calcination [46]. The detailed mineralogical composition of cement, calcined clay and limestone obtained by X-ray fluorescence (XRF) analysis was reported in a previous investigation by Wang et al. [47, Table 2]. It is worth noting that the calcined clay features silica (SiO_2) and alumina ($Al2O_3$) contents of 50.2%

Table 1
Mix design of the two SHCC mixtures under investigation.

Raw material	Product|Supplier	FA [kg m^{-3}]	LC^3 [kg m^{-3}]
Cement	CEM I 52.5 R-SR3/NA, Holcim GmbH, Germany	567	594
Fly ash	Steament® H-4, EP Power Minerals GmbH, Germany	569	–
Calcined clay	Liapor GmbH & Co.KG., Germany	–	378
Limestone	Saxodol®, SH minerals GmbH, Germany	–	189
Calcium sulphate	$CaSO_4 * \frac{1}{2}H_2O$, Honeywell International Inc., Germany	–	30
Quartz sand	BCS413, Strobel Quarzsand GmbH, Germany	536	536
UHMWPE fibres	Dyneema® SK60, 6 mm, EuroFibers BV, The Netherlands	20	20
Superplasticiser	MasterGlenium ACE 460, MBCC Group, Germany	11	12
Viscosity modifying agent	UW Compound-100, Sika AG, Switzerland	2	2
Water	–	344	358

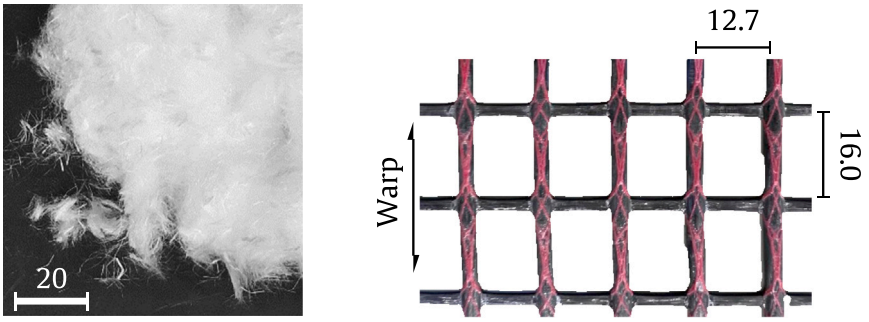

(a) PE fibres (b) Carbon textile

Fig. 2. Geometry and appearance of PE fibres and carbon textile [dimensions are in mm].

and 25.6%, respectively, while limestone is composed of calcite (54%) and dolomite (44%) [48]. Both mortars contain an extremely fine-grained quartz sand (diameter range between 0.06 and 0.2 mm) as the inert phase, and the rheological properties are controlled through the addition of a polycarboxylate-based superplasticiser admixture and a viscosity modifying agent consisting primarily of calcium carbonate ($CaCO_3$).

2.1.2. Fibre and textile reinforcements

To impart a strain-hardening attitude to the mortars, ultra-high molecular weight polyethylene (UHMWPE, hereafter referred to as PE) fibres are used, possessing length of 6 mm, see Fig. 2a. The optimum fibre volume fraction is set at 2% [49].

The PE fibres feature nominal diameter of 20 μm, tensile strength and elongation of 3000 MPa and 3.5 %, respectively, and modulus of elasticity of 103 GPa [50]. To manufacture textile-reinforced (TR)-SHCC hybrid specimens, a non-crimp biaxial unbalanced carbon textile specifically designed for structural strengthening is employed (SITgrid040, Wilhelm Kneitz Solutions in Textile GmbH, Germany). The textile is characterised by an open mesh to facilitate matrix interlocking through the different layers, and the yarns are impregnated with polyacrylate, to impart a quasi-monolithic response to the textile via promoting a more uniform stress distribution across the cross section [51]. The mesh geometry is shown in Fig. 2b, and the warp and weft directions are characterised by 3200 and 800 tex, respectively.

2.2. Specimen manufacturing and testing methods

2.2.1. Mixing protocol of the SHCC matrices

The SHCC matrices are mixed in an Eirich intensive mixer with a capacity of 25 dm^3. The mixing process is designed to avoid any undesirable agglomeration and consists of 4 steps. First, the powder phases (binder constituents and sand) are added in stages and dry mixed at 20 rpm until a uniform distribution is achieved. Second, a fluid slurry is obtained by adding water and superplasticiser and mixing at 100 rpm for 3 min and at 200 rpm for 2 min. The PE fibres are then slowly dropped into the slurry and mixed for 10 min to achieve a good dispersion before a final session of 2 min at 300 rpm before casting.

2.2.2. Uniaxial quasi-static tensile tests

The two SHCC compositions are subjected to uniaxial tensile tests on dumbbell shaped specimens in a quasi-static loading regime [52]. The total length of the specimen is 250 mm. The gauge length in the central portion is 100 mm, consisting of a 24 × 40 mm^2 cross section. At the edges, a thicker section of 40 × 40 mm^2 is realised to facilitate clamping. The reduction in the

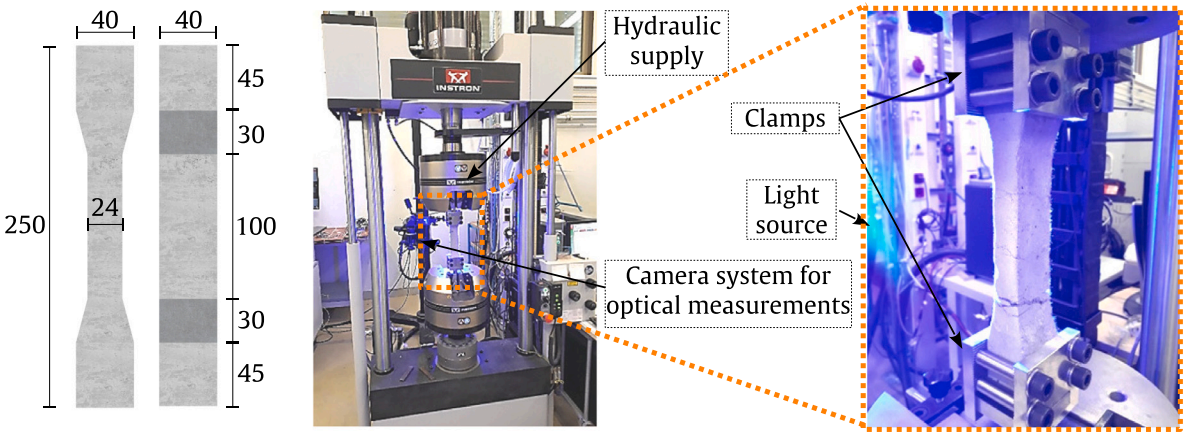

Fig. 3. Quasi-static uniaxial tensile tests on SHCC samples: specimen geometry (dimensions in mm) and test set-up.

cross-section is progressive to avoid abrupt changes in stiffness and to prevent localised cracks in the specimen at the end of the grips. The specimen geometry is detailed in Fig. 3. The fresh SHCC mixes are poured into purpose-built steel moulds, properly lubricated, and air bubbles are made emerge by mechanical jolting.

Tests are performed on an Instron 8802 universal testing machine at a displacement rate of 0.05 mm/s. The specimen is clamped at both edges by a rigid steel cage, and lateral pressure is applied by a series of bolts, to prevent undesired slippage and rotation during the test. The actual strain along the gauge length of the specimen is measured using virtual strain-gauges applied on an optical system (Digital Image Correlation - D.I.C. - GOM Aramis, Carl Zeiss GOM Metrology GmbH). To this aim, one side of the specimen is speckled with a high contrast stochastic pattern.

2.2.3. Impact tests on plates

The plates for the impact tests are cast in special wooden formworks of 61 × 61 × 3 cm^3. The moulds are well lubricated to facilitate the removal of the plates. The production process is concisely described below:

- For SHCC plates, the fresh mix is poured into the mould to its full thickness (3 cm) and levelled with a trowel to favour uniform fibre orientation along the two planar directions.
- For 2-ply crossed TR-SHCC plates, a first SHCC layer of 10 mm is poured into the mould and levelled with a trowel. The textile is laid and gently pressed. A second 10-mm layer of SHCC matrix is then cast on top, and the second cut-to-size textile is applied orthogonally. A total of 4000 tex is obtained for each orientation (i.e. 0° and 90°). The final over-coating is eventually cast up to the total thickness of the mould. To ensure the correct placement of the textiles, a customised plastic leveller is made to flatten the surface to the required depth.
- When the casting is complete, the fresh sample is covered with a wet cloth and wrapped tightly in a plastic bag to ensure moist-curing.

After 24 h, the edge frame of the mould is disassembled, the plates are stripped, again covered with a wet cloth and wrapped into a plastic bag to prevent water evaporation that could cause premature cracking. The plates are then stored in a climatic chamber at 20°Celsius for a minimum curing period of 28 days (total), before the impact tests are performed.

The impact experiments are carried out on the drop-tower facility at the Otto Mohr Laboratory of the TU Dresden. The test device is set up in a controlled accelerated configuration. The impactor is propelled by compressed air through a steel tube to hit the specimen from a height of approximately 11 m. The composite plates are fixed to a steel frame by a series of steel bolts to provide restraint on all sides (see Fig. 4). An 8.4 kg steel impactor with a diameter of 100 mm and a length of 150 mm is used. The ratio of plate thickness to impactor diameter (H/d) is 0.3.

The impactor tip is rounded to a radius of 200 cm to impart a uniform stress distribution underneath [53]. Different values of test pressure are selected as input, as described below. The actual impact velocity (v_1), the residual velocity (v_2) values, and the deflection of the upper plate surface are measured directly by using a photogrammetric technique consisting of a high-speed stereo cameras system (HSC, see Fig. 5a-b) with a frame rate of 5000 fps. The residual displacement of the plate in the immediate vicinity of the impact location, where no image correlation is possible due to the destructive nature of the test, is measured with a ruler after the test (see Fig. 5c).

The kinetic energy values $E_{kin,1}$ and $E_{kin,2}$, corresponding to v_1 and v_2 respectively, as well as the energy differences ΔE_{kin} are determined using Eqs. (1) and (2). The energy values are crucial parameters to quantify the damage tolerance and dissipation ability of the composite plates under investigation.

$$E_{kin,i} = \frac{m}{2} \cdot {v_i}^2 \tag{1}$$

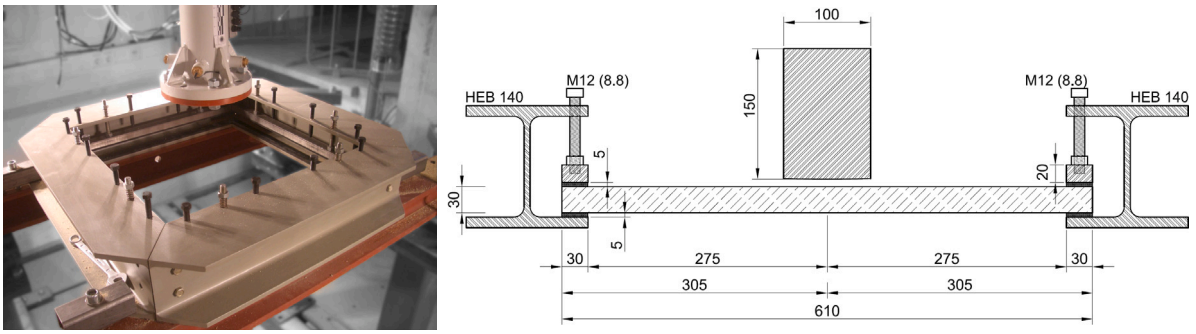

(a) Support frame (b) Cross section of test setup [mm]

Fig. 4. (a) Test set-up for impact tests and (b) a schematic view of the clamping configuration [53].

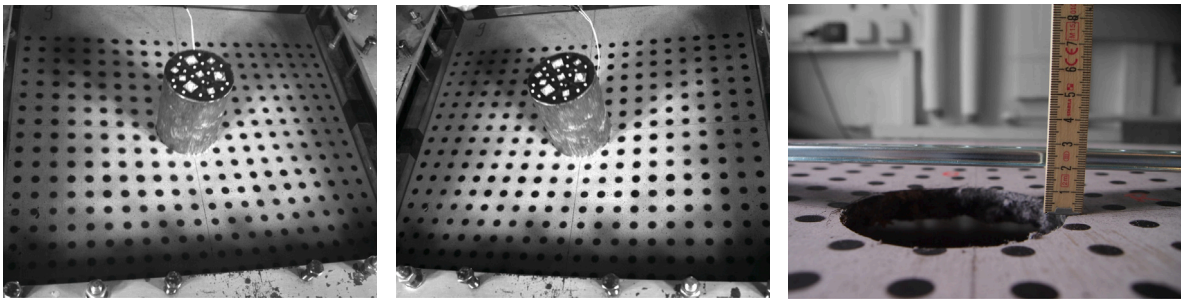

(a) Left HSC (b) Right HSC (c) u_{res} in the crater

Fig. 5. (a,b) Single frame of stereo high-speed camera recording during the impact experiment and (c) manual measurement of the residual displacement near the impact crater using a ruler.

Table 2
Impact velocity matrix.

Specimen group	$v_{bl,e}$ [m/s]	$v_{1,a}$ [m/s]	$v_{1,b}$	$v_{1,c}$	$v_{1,d}$	$v_{1,e}$	$v_{1,f}$
FA-SHCC LC3-SHCC	22–27	19	22	–	29	31[a]	–
FA-TR-SHCC LC3-TR-SHCC	27–31	–	–	25	29	31	37[a]

[a] Indicates three replicates.

$$\Delta E_{kin} = E_{kin,1} - E_{kin,2} \tag{2}$$

In Eq. (1), v_i is the velocity of the projectile, where the index i can be either 1 (input) or 2 (residual), while m is the mass of the impactor.

One of the objectives of this study is to determine the ballistic limit for the different material combinations being considered. This is done by testing six specimens for each material combination. The input velocity is varied gradually in order to obtain all possible damage modes. In addition, perforation failure is tentatively targeted on a minimum of four specimens within each group. Although significant differences in the mechanical behaviour of the plates are expected depending on the presence of textile reinforcement, as many input velocity levels as possible coincide across the different sets of specimens. This approach enables a comparative assessment of the extent of damage for different material combinations under the same loading condition. After the tests, the damage is documented photographically, the fracture body portions are analysed and the residual plate masses are determined. Indeed, the loss of mass is one of the indicators of the impact safety of strengthening materials, together with the average debris size. Table 2 summarises the experimental matrix, and indicates the four test input velocities that were selected for each of the sample groups.

FA and LC^3 refer to the two different binder compositions, including fly ash and limestone calcined clay, respectively. To fine-tune the test conditions, the expected penetration limit ($v_{bl,e}$) is empirically estimated based on damage assessment of previous experiments reported by Hering [53].

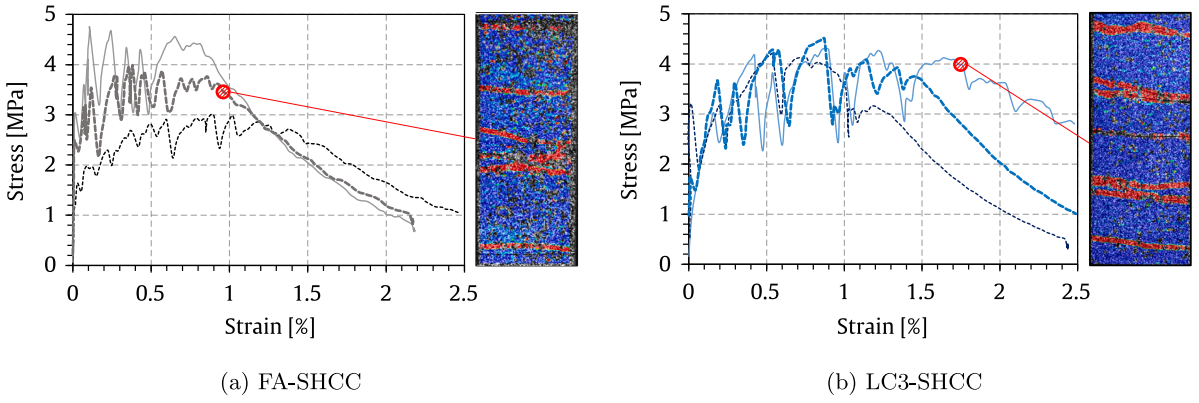

Fig. 6. Stress–strain curves showing the tensile behaviour of the SHCC formulations. The crack patterns of two typical specimens recorded at the onset of softening are also shown.

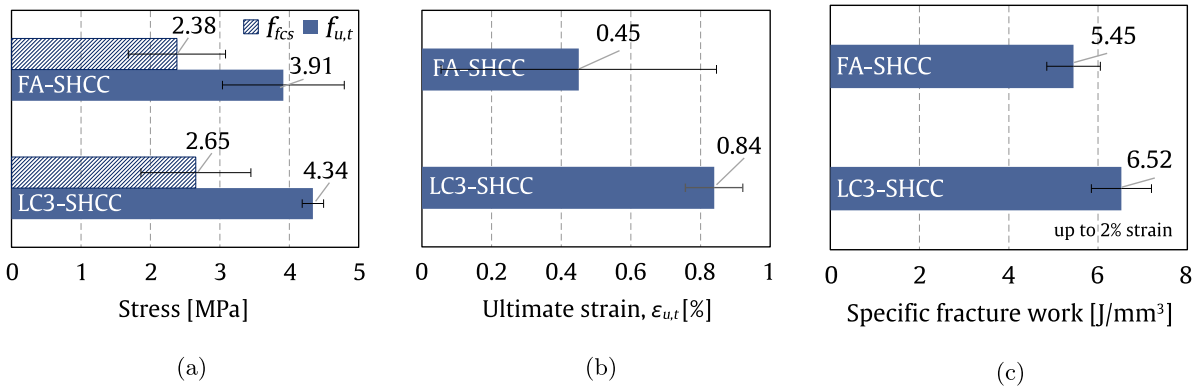

Fig. 7. Bar charts reporting on the tensile parameters of the SHCC matrices. Standard deviation bands denote data scatter.

3. Results and discussion

3.1. Quasi-static uni-axial tensile tests

Fig. 6 shows the tensile behaviour of FA-SHCC and LC^3-SHCC under a quasi-static load regime, along with the crack pattern measured in terms of axial strains at the onset of the softening branch.

Three dumbbell specimens are tested for each binder formulation. Both composites exhibit pronounced strain hardening, i.e. consistent increase in stress is achieved after matrix cracks, as a result of effective crack bridging and stress transfer that are exerted by the PE fibres. It is worth noting that while the peak stress is only slightly affected by the substitution of fly ash with limestone and calcined clay as SCMs in the blended binder, some gain in strain capacity is observed for LC3-SHCC.

Fig. 7 displays the main performance indices that qualify the mechanical response of the SHCC matrices under quasi-static loading. The evaluation of first cracking stress (f_{fcs}) and tensile strength ($f_{u,t}$) quantifies the extent of strain hardening exhibited by the SHCC matrices (see Fig. 7a). The ultimate strain ($\varepsilon_{u,t}$, also referred to as the *strain capacity*) is regarded as the strain corresponding to the attainment of the tensile strength (see Fig. 7b). The strain capacity in combination with the specific fracture work (W) absorbed up to 2% of the strain, showed in Fig. 7c, effectively reports the ductility and damage tolerance of SHCC. W is obtained as the normalised mechanical work per unit volume (V_G), i.e. divided by $V_G = A \cdot L_G$, where A and L_G are the cross-sectional area and gauge length of the dumbbell specimen, respectively. FA-SHCC features a tensile strength of 3.9 MPa, combined with a strain capacity of about 0.45%, whereas the composite based on the LC^3 binder is characterised by a tensile strength of 4.3 MPa and a strain capacity of about 0.84%. In addition, the standard deviation associated with the strength of LC3-SHCC is lower. It is also worth noting that the average strain values prior to the onset of the final softening branch, corresponding to the final damage clustering, are approximately 0.98% and 1.32% for FA-SHCC and LC3-SHCC, respectively. These results are consistent with previous data where PE fibres were adopted in combination with fine-grained cementitious mortars [54]. Although the strain capacity of the presented SHCC under quasi-static tensile loading is lower than that of other studies involving hydrophilic fibres, e.g. polyvynylalcohol (PVA), the given formulations are chosen because a remarkable enhancement in micromechanical properties is expected at high strain rates,

Table 3
Test results for SHCC and hybrid plates subjected to accelerated drop-weight impact loading.

Label	v_1	v_2	ΔE_{kin}		Δm_{plate}		Failure mode
	[m/s]		[J]	[%][a]	[kg]	[%][a]	
FA-SHCC1	18.91	−3.59	1448.37	96.40	0.04	0.19	Reb.
FA-SHCC2	21.86	7.71	1757.74	87.55	0.74	3.82	Perf.
FA-SHCC3	28.21	20.82	1522.58	45.54	0.82	4.09	Perf.
FA-SHCC4	28.56	14.39	2554.92	74.60	0.84	3.72	Perf.
FA-SHCC5	30.64	21.52	1996.48	50.64	0.88	4.16	Perf.
FA-SHCC6	31.49	24.16	1712.36	41.12	0.76	3.85	Perf.
FA-TR-SHCC1	24.84	−3.57	2538.08	97.94	0.06	0.31	Reb.
FA-TR-SHCC2	29.27	0.00	3598.28	100.00	0.40	2.06	Pen.
FA-TR-SHCC3	30.26	9.01	3504.25	91.14	0.62	3.12	Perf.
FA-TR-SHCC4	36.43	21.70	3597.29	64.53	0.74	3.57	Perf.
FA-TR-SHCC5	36.46	19.23	4029.52	72.17	0.72	3.43	Perf.
FA-TR-SHCC6	37.29	23.15	3589.81	61.46	0.74	4.12	Perf.
LC3-SHCC1	19.14	−3.66	1483.00	96.35	0.00	0.00	Reb.
LC3-SHCC2	22.46	1.27	2111.92	99.68	0.88	4.31	Perf.
LC3-SHCC3	28.79	20.97	1633.73	46.93	0.70	3.28	Perf.
LC3-SHCC4	29.75	23.13	1470.92	39.57	0.80	3.92	Perf.
LC3-SHCC5	30.84	19.71	2363.87	59.16	0.72	3.36	Perf.
LC3-SHCC6	32.42	23.87	2022.28	45.80	0.78	3.65	Perf.
LC3-TR-SHCC1	25.74	−4.24	2707.80	97.28	0.02	0.09	Reb.
LC3-TR-SHCC2	28.53	0.00	3417.84	100.00	0.04	0.19	Pen.
LC3-TR-SHCC3	32.11	10.15	3898.34	90.00	0.24	1.17	Perf.
LC3-TR-SHCC4	37.43	20.64	4093.35	69.58	0.96	4.38	Perf.
LC3-TR-SHCC5	37.93	23.93	3638.04	60.21	0.56	2.90	Perf.
LC3-TR-SHCC6	38.48	23.51	3897.14	62.68	0.90	4.35	Perf.

[a] Related to $E_{kin,1}$ and $m_{plate,1}$.
Reb. = rebound; Pen. = penetration; Perf. = perforation.

i.e. impact, as demonstrated by the dramatic dynamic increase factors (DIFs) measured in terms of fibre–matrix bond by Trindade et al. [55]. This strain sensitivity is reflected in an improved response of PE-SHCCs compared to their PVA counterparts [56].

Comparing the performance indices in Fig. 7, LC3-SHCC consistently outperforms the reference composite in terms of strength and ductility, with a pronounced strain hardening ratio ($f_{u,t}/f_{fcs}$) of (1.77 ± 0.70), which appears to be slightly higher than that of its FA-SHCC counterpart, i.e., (1.67 ± 0.14). However, a larger data set is required to demonstrate a robust statistical difference in the mean values.

3.2. Impact tests

Table 3 reports on the experimental data obtained in the impact tests conducted on plates. For each plate, the actual values of striking (input) and residual velocities (v_1 and v_2) are reported, in addition to the absorbed energy (ΔE_{kin}), mass loss (Δm_{plate}), and failure mode. The tests are sorted in ascending order by input velocity.

The SHCC and hybrid composite plates under investigation are compared with plain concrete (here labelled “Ref-PC”) and textile reinforced concrete (here labelled “Ref-TRC”) from previous tests using a matrix of high-strength fine-grained concrete (TF10, PAGEL Spezial-Beton GmbH & Co. KG, Germany). Again, 2-ply crossed SITgrid040 carbon textiles were used in Ref-TRC experiments [26]. These results are recalled and presented in a consistent format in Table 4.

As envisioned, for each group of samples, one plate undergoes to rebound and at least four attain full perforation. It is noteworthy that penetration is achieved experimentally for both TR-SHCC varieties. On the contrary, no penetration is obtained for the SHCC samples. However, the estimation of the second test velocity proves to be very close to the ballistic limit, as the energy differences of 87.55% and 99.68% are very close to the case of complete absorption (100%), especially for the LC3-SHCC group. In this regard, the fine quantification of the penetration/ballistic limit is related to analytical estimates based on the concept first proposed by Liu et al. [31] and validated in the practical approach recently developed by Hering et al. [42], as presented and substantiated in Section 3.2.2.

The absolute value of the ratio of residual to impact velocity ($|v_2/v_1|$) is calculated and analysed to assess the behaviour of the plates in the rebound domain. As far as the hybrid plates are considered, 14.4 % and 16.5 % of the initial velocity is reflected after impact for FA-TR-SHCC1 and LC3-TR-SHCC1, respectively. For the FA-SHCC1 and LC3-SHCC1 specimens this ratio increases to 19.0 % and 19.1 %, respectively. A comparison between these values is possible as they are associated with the same extent of absorbed energy (ΔE_{kin}), of about 97 %. On the basis of this evidence, it is reasonable to conclude that SHCC plates exhibit less plasticity than their hybrid counterparts, as a higher portion of the incident velocity is retained after impact. Unfortunately, the available data do not allow a meaningful comparison with the reference specimen Ref-TRC1, due to a different energy absorption range (ΔE_{kin} = 83.34 %).

Table 4
Test results for reference plates including fine-grained concrete matrix subjected to accelerated drop-weight impact loading.
Source: Adapted from [53].

Label	v_1	v_2	ΔE_{kin}		Δm_{plate}		Failure mode
	[m/s]		[J]	[%][a]	[kg]	[%][a]	
Ref-PC1	12.15	9.18	266.07	42.91	0.80	3.50	Perf.
Ref-PC2	12.31	9.18	282.51	44.39	0.96	3.84	Perf.
Ref-PC3	16.53	13.12	424.65	37.00	1.10	4.81	Perf.
Ref-PC4	19.68	15.65	598.00	36.76	1.76	7.06	Perf.
Ref-PC5	20.30	16.54	581.78	33.61	1.52	6.50	Perf.
Ref-PC6	24.71	20.84	740.37	28.87	1.68	7.39	Perf.
Ref-PC7	25.17	21.28	758.90	28.52	1.64	6.91	Perf.
Ref-PC8	27.95	23.07	1045.71	31.87	2.52	9.73	Perf.
Ref-PC9	33.56	27.88	1465.71	30.99	2.54	10.05	Perf.
Ref-PC10	43.60	37.92	1944.74	24.36	2.24	9.15	Perf.
Ref-TRC1	9.48	−3.87	314.55	83.34	0.26	1.11	Reb.
Ref-TRC2	21.13	9.67	1482.47	79.06	2.22	9.55	Perf.
Ref-TRC3	21.19	11.72	1308.96	69.41	2.24	9.40	Perf.
Ref-TRC4	26.13	15.13	1906.21	66.47	2.46	10.13	Perf.
Ref-TRC5	27.32	17.79	1805.57	57.60	1.72	7.21	Perf.
Ref-TRC6	33.82	26.77	1794.07	37.35	1.80	7.61	Perf.

[a] Related to $E_{kin,1}$ and $m_{plate,1}$.
Reb. = rebound; Pen. = penetration; Perf. = perforation.

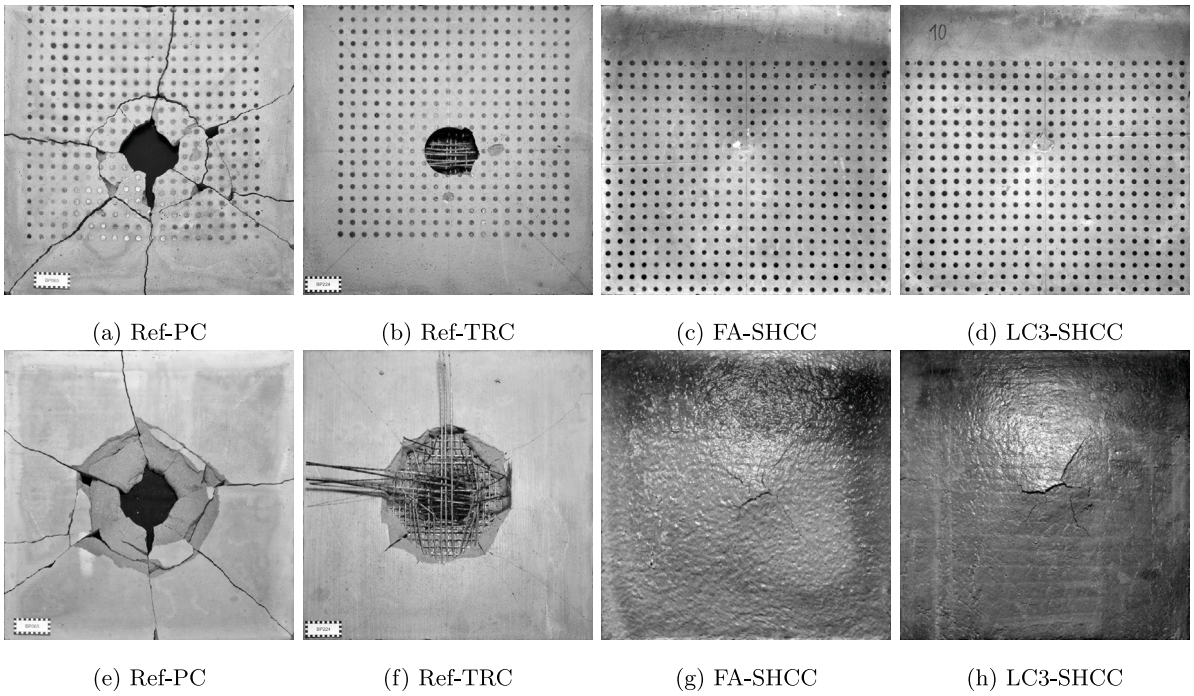

Fig. 8. Typical appearance of the front (upper row) and rear (lower row) side of composite plates tested at $v_1 = (20 \pm 2)$m/s.

3.2.1. Failure modes and damage assessment

In order to assess the extent of damage after the impact tests, all plates and fracture bodies are visually analysed and compared. Specifically, to pinpoint the effects of the addition of short fibres to cement-based mortars, Fig. 8 (inlets a-d) showcases the impacted face of the SHCC samples (c and d) compared to the Ref-PC and Ref-TRC counterparts (a and b, respectively) at the fixed striking velocity of approximately 20 m/s. The same plates are also shown on the rear side in Fig. 8 (inlets e-h).

The reference samples are completely perforated, and present a distinct circular hole on the impacted side, as a consequence of abrupt shredding of the brittle matrix. In the case of the TRC plate, the embedded textile is not activated until the concrete layer facing the impactor is completely fractured and the bond with the textile is compromised by the propagation of the shock wave. A similar failure mode was documented by Gopinath et al. [57]. Conversely, the fibres in the SHCC matrix successfully act as stitching elements for the cracks forming on the impacted side. This favourable mechanism has the twofold effect of preventing any spalling

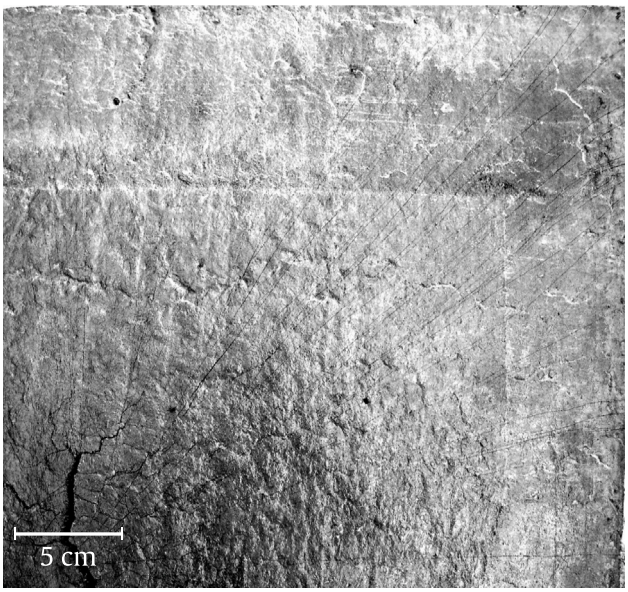

Fig. 9. Magnified view of the crack pattern of the LC3-SHCC plate of Fig. 8h. Note: The plate is sprayed with water and the image is converted to grey scale with increased contrast for better visualisation.

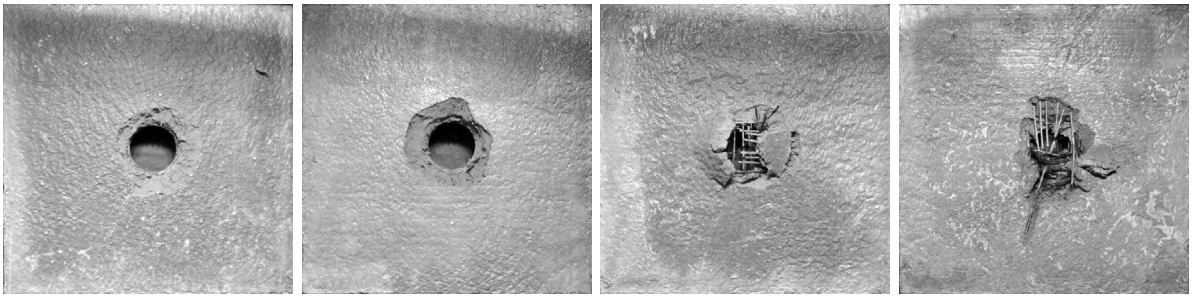

Fig. 10. Typical appearance of the rear side of composite plates tested at $v_i = (31 \pm 2)$m/s.

of the matrix in SHCC specimens and preserving the bond with the textile reinforcement. The indentation produced by the impactor is clearly visible, associated with irreversible deformation near the barycentre of the plates, resembling the typical behaviour of ductile materials.

Moving on to the visual analysis of the backsides of the aforementioned plates, few and large radial cracks trigger for Ref-PC plates, resulting in concrete scabbing and the complete destruction of the plate. Although a similar crack pattern occurs in the Ref-TRC plates, the internal textile layers demonstrate the ability to absorb some of the impact energy, resulting in significantly smaller crack widths. Upon failure, the plate is held together by yarn interlocking. However, a considerable portion of the plate fragments are ejected after the collision. In the SHCC specimens, cracks initiate and propagate on impact, but the sewing action of the fibres fosters effective smearing of the damage across the entire specimen surface. This is also visible in the enlarged view of the LC3-SHCC plate quarter (Fig. 8h) shown in Fig. 9, where a diffuse radial crack pattern can be observed.

This phenomenon of multiple crack branching allows for significant dissipation of mechanical energy deriving from the impact, retarding perforation more effectively than in the case of textile alone, and mitigating scabbing of matrix debris. Again, it should be noted that irreversible damage is widespread on the rear side of the SHCC plates, contrarily to the brittle cementitious matrix counterparts without fibres. Similar observations on the craters on the impact far side were also experienced in the investigation of ultra-high performance steel fibre-reinforced concrete; see Máca et al. [58]. From this qualitative damage assessment, the effects of different binders (namely FA and LC^3) cannot be visualised. To appraise the contribution of the addition of textile layers to the impact behaviour of the composite plates, the typical appearance of SHCC and TR-SHCC samples (rear side) is compared in Fig. 10 at an impact velocity of approximately 31 m/s.

Fine cracks are not plainly visible at higher impact velocities in vicinity of the impactor imprint. Indeed, these portions of the plate are subjected to severe localised shear and if the perforation limit is amply breached (as in the case of SHCC in Fig. 10), a

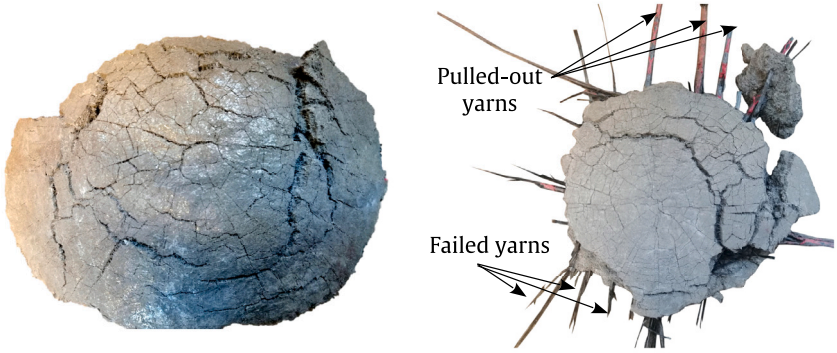

Fig. 11. Far side of the punching cone ejected from perforated plates.

more brittle shear response is expected, owing to the tensile failure of the PE fibres [56]. The addition of textiles imparts further reinforcement to the matrix and, combined with the dissipative attitude of the short fibres, enhances the integrity of the SHCC matrix during severe impact regimes. As a result, the operational textile-to-SHCC bond is maintained to some extent, improving the composite toughness [59].

Fig. 11 shows the back side of the fracture cones for perforated LC^3-SHCC and corresponding hybrid plates.

The radial crack pattern triggered under severe bending can be nicely observed for both composites. Aligned fibres effectively bridging the major cracks in the SHCC matrix can also be seen with the naked eye. The shape of these cones is significantly deformed, as an indicator of irreversible damage due to multiple cracking that largely contributes to energy dissipation. In the case of the hybrid composite, the textile failure is mixed. Some yarns are sharply truncated by abrupt fibre failure, due to high tension and/or shear, whereas some other bundles appear to be clearly pulled out, as also documented by the polyacrylate coating being scratched out due to severe friction. This evidence clearly emphasises the critical role played by yarn-to-SHCC bond and the paramount importance of tuning the chemical and mechanical interactions between the phases as a function of the expected strain rate of the external load [60,61].

3.2.2. Energy dissipation and ballistic limit

To quantitatively determine the toughness of the different composite plates, the dissipated kinetic energy (ΔE_{kin}) is plotted as a function of the input kinetic energy ($E_{kin,1}$) in the graphs in Fig. 12. On the left hand side (inlets *c* and *e*), SHCC plates without textile reinforcement are considered and compared with the plain concrete benchmark (inlet *a*). On the right hand side (inlets *d* and *f*), TR-SHCC plates are compared with the reference TRC (inlet *b*). The markers are representative of the experimental results, while the bilinear fit is determined according to Hering et al. [42]. The first straight line (black, solid) identifies the equal-energy limit condition, where all the impact energy is absorbed by the target, i.e. the bisector of the $E_{kin,1} - \Delta E_{kin}$ diagram (see Eq. (3)).

$$\Delta E_{kin} = E_{kin,1} \tag{3}$$

For the lowest input energy values, the composite plate is able to absorb most of the impact energy. The residual kinetic energy of the impactor is either 0, in the case of perfect penetration, or very low, as limited input velocities are involved. In fact, residual energy upon rebound is about 2%–3% of the corresponding input energy (see Table 3), so the test points deviate slightly below the equal-energy limit. With increasing v_1 values, perforation occurs and the experimental points deviate distinctly from the equal-energy threshold. The energy absorption ΔE_{kin} tends to increase slightly at increasing input energy values $E_{kin,1}$ and the inherent relationship is well interpreted by a linear fit, with a slope ranging from 0 to 8% (for SHCC and TR-SHCC) and from 14% to 23% (for reference tests) with respect to the bisector. This flattened trend is in line with the findings by Liu et al. [31] for polymer-based laminates. The intersection of the two mentioned straight lines leads to the inference of the limit energy $E_{kin,bl}$, which can be considered as a material feature for thin composite plates in this test configuration. The corresponding penetration velocity v_{bl} can be retrieved by inverting Eq. (1).

The validity of this analytical approach is affirmed by experimental evidence for TR-SHCC plates, for which penetration was experimentally attained (void circular markers in Fig. 12d and f). In is noteworthy that the relative discrepancy between experiment and prediction is below the 5% threshold for both hybrid composites. According to this method, the ballistic limit for a given material combination can be obtained by conducting experiments only in the perforation domain, given the hypothesis of small H/d ratios mentioned in the introductory section. Indeed, while for thick slabs the damage scenarios for a given input energy are highly sensitive to the impactor size, mass and velocity [62], in the present case, the H/d ratio is 0.3, thus falling in a range where the plate response is mainly driven by inherent material properties, and structural effects related to the plate geometry, are minimised [41,63].

Once the validity boundaries of the current investigation have been established, the ballistic limit energy values are visually represented in orange colour in the comparative chart in Fig. 13, obtained as the abscissa of the transition points in Fig. 12 (red dash-dotted lines).

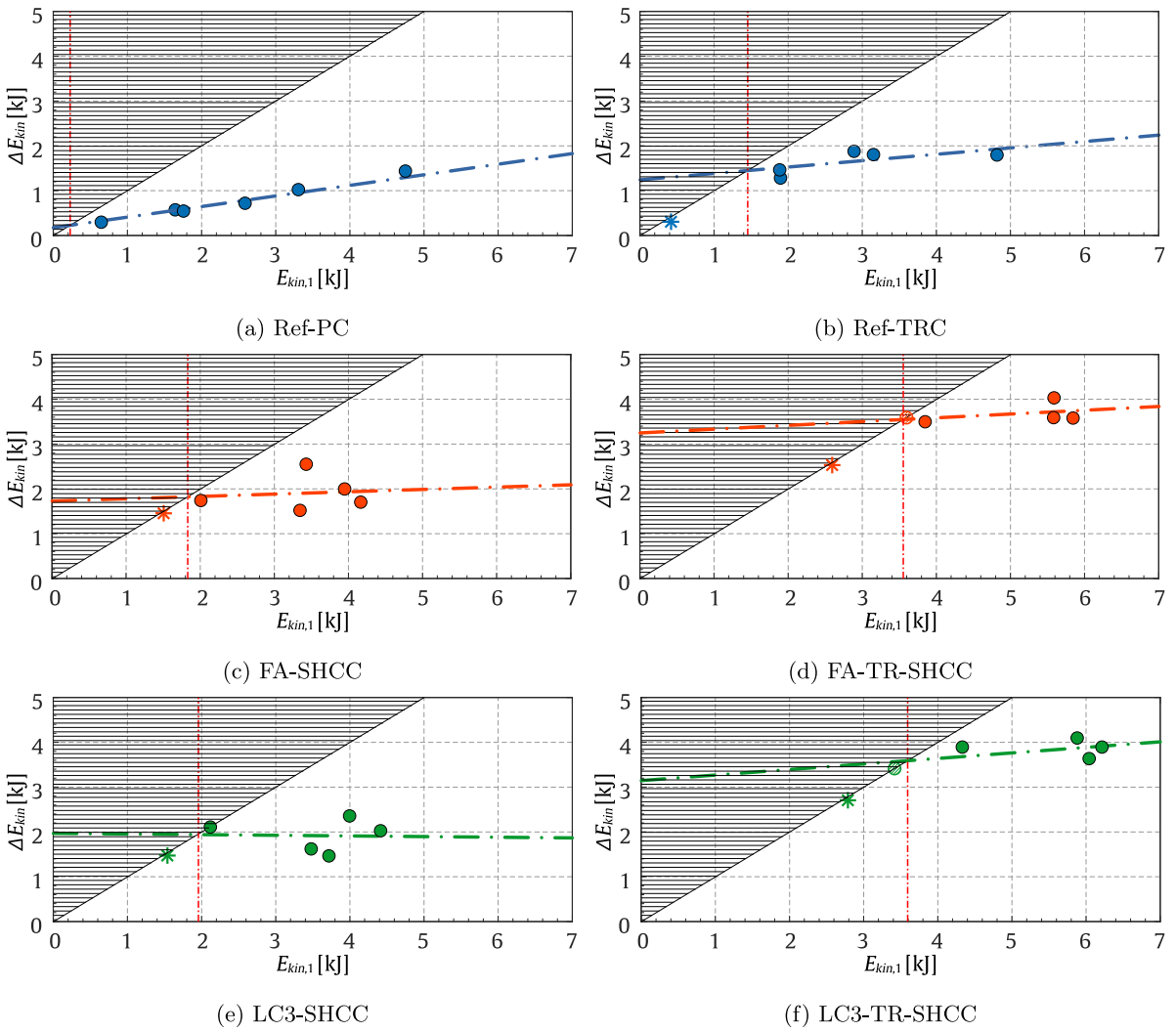

Fig. 12. Energy dissipation capability of the tested plates in terms of $E_{kin,1} - \Delta E_{kin}$ diagrams. The "equal-energy" domain (bisector) is marked with a solid black straight line. The hatched areas above this limit represent a non-physical disregarded domain. Dash-dotted lines represent the linear fitting of experimental points associated with perforation failure (solid-coloured circles). Rebound experiments are plotted with asterisks, and penetration experiments with void circles.

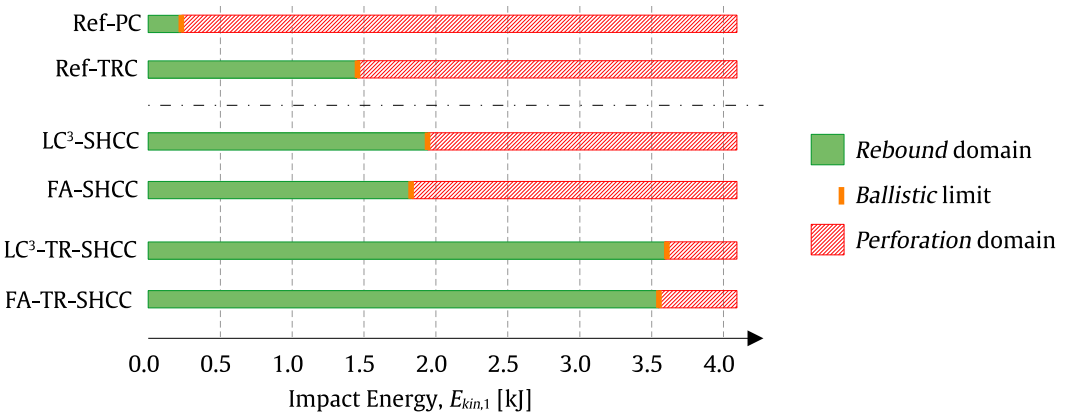

Fig. 13. Comparative evaluation of the impact behaviour of SHCC and hybrid composites in terms of the ballistic limit, as defined by Hering et al. [42]. Reference values from previous tests on plain fine-grained concrete and corresponding TRC are reported [26].

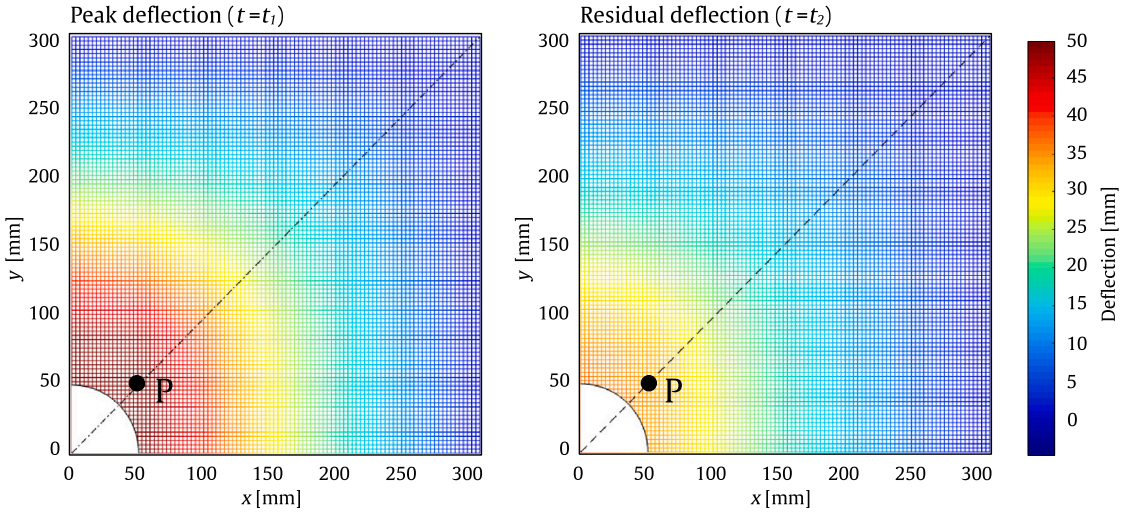

(a) $v_1 = 21.9\,\mathrm{m/s}$ (LC3-SHCC2)

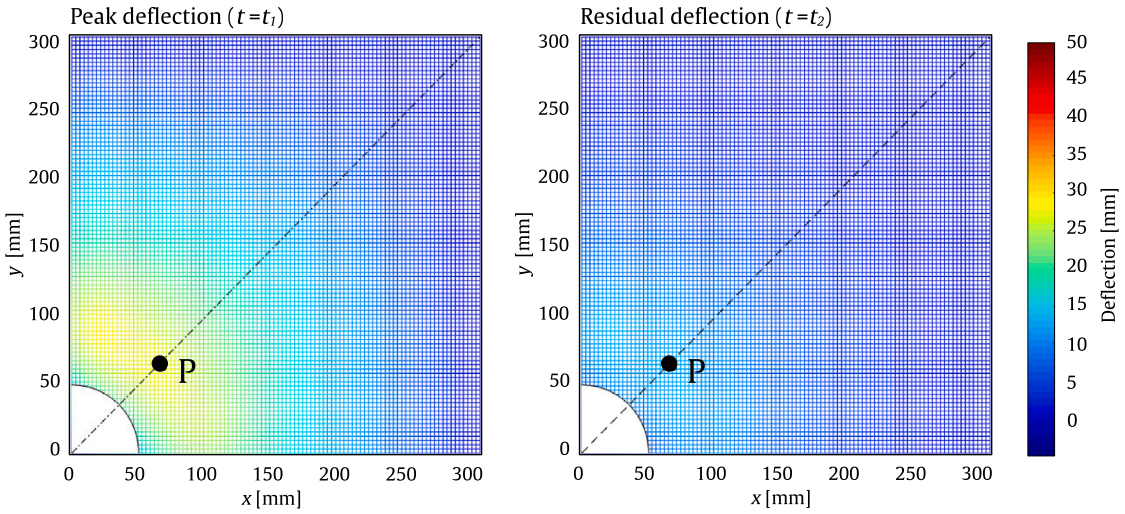

(b) $v_1 = 32.2\,\mathrm{m/s}$ (LC3-SHCC6)

Fig. 14. Deflection field computed with DIC measurements for LC3-SHCC at two different failure modes: (a) perforation very close to the penetration limit, and (b) perforation far from the penetration limit. *P* indicates the selected point to monitor the deflection vs time in Fig. 15.

All the composite plates tested in the current study feature higher ballistic limit than the Ref-PC and Ref-TRC counterparts, where no dispersed fibres are considered in the mix design. Remarkably, the beneficial contribution supplied by the dispersed fibres outweighs that brought in by the textiles alone. Indeed, the perforation threshold for the SHCC samples is ascertained to be 26% and 34% higher than that of the plain TRC counterparts, when FA and LC^3 binders are considered, respectively. As envisioned in Section 3.2.1, this substantial enhancement in impact performance can be traced back to the attitude of the fibres to dissipate energy by inducing a favourable fine crack pattern [64]. Conversely, in plain TRC, the concrete matrix undergoes a brittle fragmentation process and the textile is subjected to sharp punching in a concentrated area. Nevertheless, the mechanical performance of the carbon textiles allows the Ref-TRC samples to record a significant improvement over plain concrete, reflected in a 5.5-fold increase in the ballistic limit. Moving on to hybrid composites, the interaction established between the short fibres and the textile reinforcement leads to remarkable increases in the perforation resistance compared to other solutions, including alternatively short or continuous fibres. In fact, the TR-SHCC samples stand out for a twofold increase in the ballistic limit compared to the corresponding SHCC, which outweighs the mere summation of the effects by about 10%. This is attributed to the increase in toughness of the matrix due to the fibres, being responsible for maintaining the bond between the matrix and the textile, and favouring a more efficient stress transfer mechanism, so that a greater portion of the textile reinforcement is activated on impact, optimising its response. Whilst failure modes do not vary significantly between the two binders (see Fig. 10), composites made with the LC^3 binder consistently

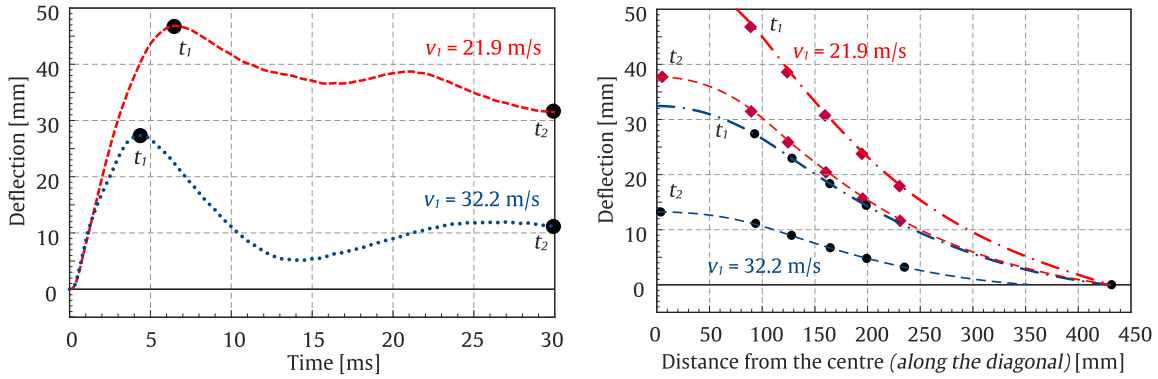

(a) Deflection vs time in P (b) Deflection vs distance to centre

Fig. 15. Temporal and spatial deflection profiles for LC3-SHCC2 (blue lines) and LC3-SHCC6 (red lines) plates. t_1 and t_2 refer to the time instants when peak and residual strain values are attained, respectively. (For interpretation of the references to colour in this figure legend, the reader is referred to the web version of this article.)

exhibit slightly higher tolerance to perforation than fly ash based counterpart, namely 6% for SHCC and 2% for TR-SHCC. This evidence, albeit minimal, is well in line with the material response in the quasi-static regime.

3.2.3. Plate deflection and irreversible damage

Fig. 14 shows the vertical displacement (deflection) maps for LC3-SHCC plates, measured at the time instants when the peak (hereafter regarded as t_1, left) and residual deflection (hereafter regarded as t_2, right) values occur. The latter is hereafter referred to as u_{res}. The measurements are taken on a plate quarter, as double symmetry is assumed. The quarter circle at the bottom left of each chart stands for the position of the impactor. Two samples are compared, namely the one closest to the penetration limit (LC3-SHCC2, inlet *a*) and the one struck at the highest impact velocity, in the far perforation domain (LC3-SHCC6, inlet *b*).

The amplitude of the deflection is not directly proportional to the impact velocity. Indeed, higher deformations are detected for the striking velocity closest to the penetration limit, as a consequence of a wider activation of the plate surface, as also observed by Corbett et al. [65]. To further elucidate this evidence, Fig. 15a plots the time histories of the displacements measured at the points marked with P in Fig. 14.

For each impact test, a peak deflection is reached, followed by oscillation of the plate. In the case of the SHCC samples, the maximum deflection is reached between 4 ms and 7 ms, and a secondary peak is generally attained at a later stage (between 20 ms and 25 ms). As expected, the higher the impact speed, the shorter the rise time. The maximum deflection at point P for the LC3-SHCC2 plate (close to the penetration limit) is about 58% higher than for the LC3-SHCC6 (far perforation). Fig. 15b compares the spatial deflection profiles measured on the plate diagonal (at the edges, the setup constraints result in nominal zero deflection) at instants t_1 and t_2. The data points are interpolated by means of *spline* polynomial functions and the area between the curves is representative of the deflection recovery capacity of the plate. In fact, the smaller the discrepancy between the peak and residual curves, the greater the irreversible deformation. By comparing the pairs of measured deflection values at t_1 and t_2 at various distances from the centre of the plate, the extent of irreversible deformation can be gauged. For the impact velocity closest to the penetration limit, most of the deflection is irreversible (about 65%), contrarily to the case of the far perforation, where most of the deflection is recovered (irreversible deformation about 35%). This finding is indicative of a close correlation between the penetration limit and the deflection of the target, as developed further hereafter.

Likewise, Fig. 16 plots the 2D colour map for the deflection fields of the LC3-TR-SHCC samples. The test velocities are sensibly higher, but the same damage scenarios, i.e., penetration and far perforation, are compared. Interestingly, only a slight reduction in peak displacement was detected when comparing SHCC and hybrid specimens at both time instants. Conversely, the residual displacements are significantly lower than the SHCC counterparts. Yoo et al. [66] also reported on a direct correlation between the extent of reinforcement and deflection recovery, albeit therein steel rebar in ultra-high performance concrete beams were studied.

In addition, Fig. 17 reports on the time history and the spatial profile of deflection for the LC3-TR-SHCC plates.

The former plot reveals that after the peak load is attained, two more relative maxima are generally reached, while the latter plot confirms that a higher fraction of the peak deflection is recovered. In fact, the irreversible portion of the peak deflection for hybrid plates is half (30%) that of the SHCC counterpart for the plate at the penetration limit, and even reduced by up to a third (14.5% on average) for the far perforation case. Accordingly, the addition of textiles promotes the global response of the specimens and the plates efficiently distribute the shock load, acting likewise as a membrane. Cross-checking these data with the plate response estimated in the rebound phase with the coefficient $|v_2/v_1|$ (see the beginning of Section 3.2), it is clear that while the TR-SHCC shows a slightly higher degree of plasticity than the SHCC counterpart at low impact energy, the trend is clearly reversed for impact loads approaching and then breaching the ballistic limit. In fact, fibres alone are not capable of activating a global behaviour of the plate at higher applied loads with the same effectiveness as continuous and rigid textile meshes.

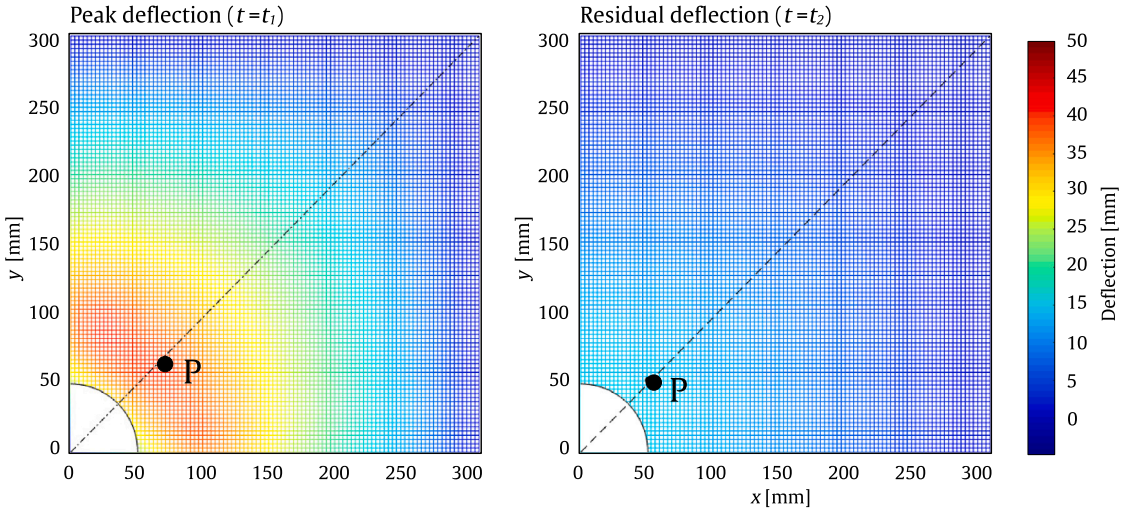

(a) $v_1 = 28.2\,\mathrm{m/s}$ (LC3-TR-SHCC2)

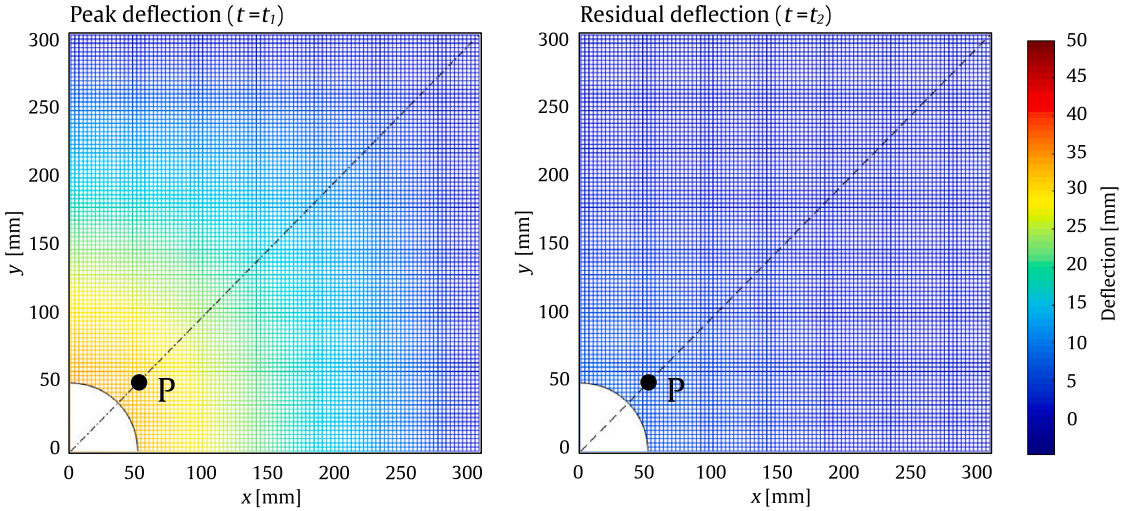

(b) $v_1 = 37.7\,\mathrm{m/s}$ (LC3-TR-SHCC6)

Fig. 16. Deflection field computed with DIC measurements for TR-LC3-SHCC at two different failure modes: (a) penetration limit, and (b) far perforation. *P* indicates the point selected to monitor the deflection vs time in Fig. 17.

To better characterise the irreversible damage on the impacted plates, and to quantify the correlation with the ballistic limit, the values of the residual deflection at the centre of the plate after the test, i.e. u_{res} are plotted in Fig. 18a. A zoomed view of the groups of specimens tested in this study is provided in Fig. 18b and c, divided by binder type.

Measurement of u_{res} was not possible for the Ref-PC specimens, due to complete shredding of the plates after the tests. A direct polynomial fitting curve is also proposed to capture the trend of u_{res}, which turns out to be a non-monotonic function of the striking velocity. Rather, it accurately resembles a cubic curve with negative concavity, having both relative maximum and minimum points within the velocity range studied. Due to the limitations of the data sets, an exception is the FA-TR-SHCC group, which deviates from the trend of all the other data sets, due to an anomaly in the rebound experiment. Nonetheless, the experimental points in the perforation stage still follow the expected decreasing trend with increasing impact velocity.

The curves in Fig. 18 are modelled on the basis of empirical assumptions, as illustrated in Fig. 19.

The boundaries of the cubic fitting domain (hereafter regarded as *transition domain*) are given on the left hand side by the intersection with the x-axis (hereafter regarded as the *elastic limit*) and on the right, by the relative minimum (hereafter regarded as the *stabilisation limit*). Outside the transition domain, two constant functions are proposed, namely the null function, assuming that no permanent deflection occurs in the elastic region, and the constant function equal to the relative minimum of the cubic fit, respectively.

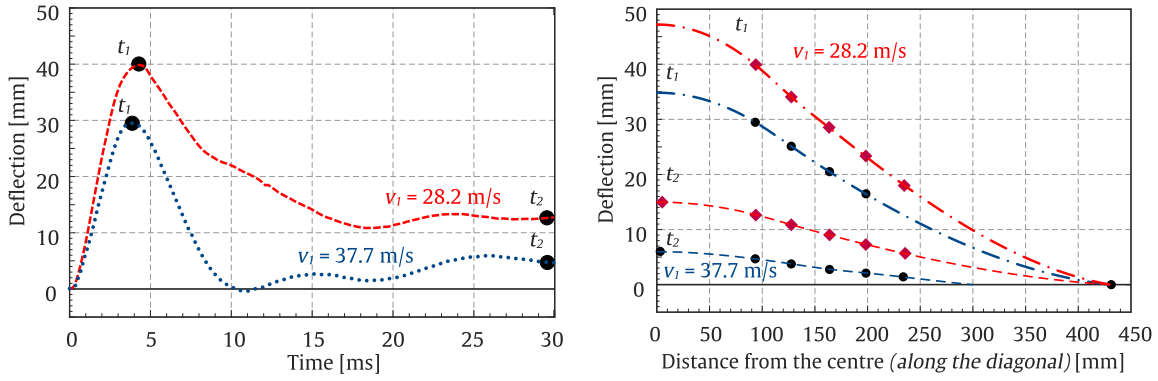

(a) Deflection vs time in P

(b) Deflection vs distance to impact

Fig. 17. Temporal and spatial deflection profiles for LC3-TR-SHCC2 (blue lines) and LC3-TR-SHCC6 (red lines) plates. t_1 and t_2 refer to the time instants when peak and residual strain values are attained, respectively. (For interpretation of the references to colour in this figure legend, the reader is referred to the web version of this article.)

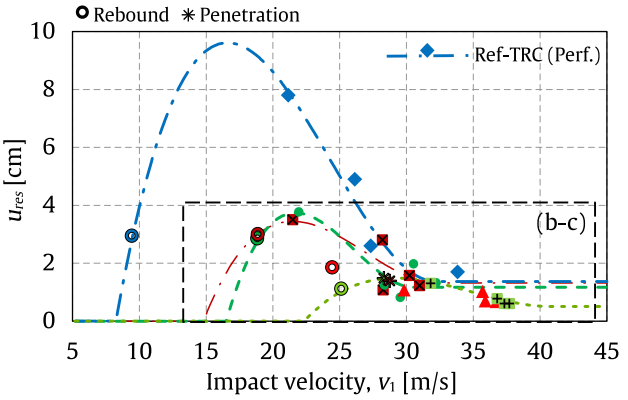

(a) All the tested samples (dashed box) compared to TRC plates (measurement of u_{res} was not possible for Ref-PC due to complete fragmentation of the plates).

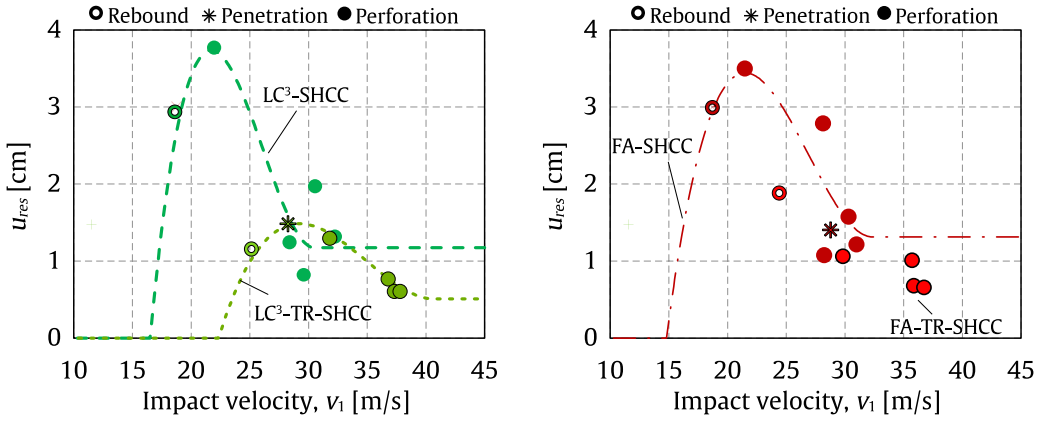

(b) LC^3

(c) FA

Fig. 18. Non-monotonic trends of the irreversible deformation values u_{res} as a function of the input velocity v_1. Fitting curves are also plotted (perforation experiments on TR-SHCC are denoted by the black contour). For FA-TR-SHCC, the fitting was not possible with the available data.

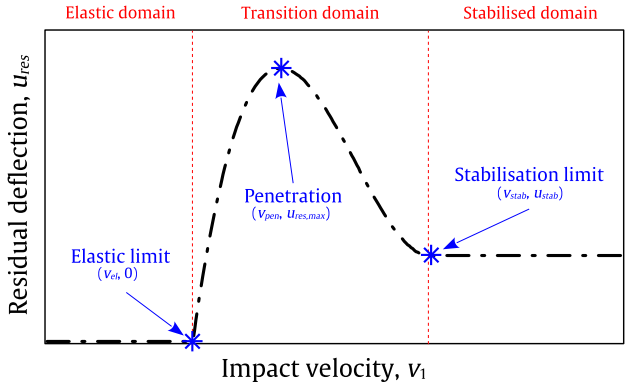

Fig. 19. Phenomenological interpretation of the $v_1 - u_{res}$ trend.

Table 5
Estimation of the ballistic limit (v_{bl}) by fitting the measured residual deflection values from the experiments.

Label	Bilinear	Residual deflection						Error
	v_{bl} [m/s]	v_{el} [m/s]	v_{bl} [m/s]	$u_{res,max}$ [cm]	R^2 [–]	v_{stab} [m/s]	u_{stab} [cm]	v_{bl} [%]
Ref-PC	7.4	–	–	–	–	–	–	–
Ref-TRC	18.6	8.30	16.60	9.61	0.96	32.19	1.37	−11.8
FA-SHCC	20.9	14.80	21.49	3.44	0.68	32.33	1.32	+2.8
LC3-SHCC	21.5	16.50	21.71	3.74	0.86	30.50	1.17	+1.0
FA-TR-SHCC	29.1	–	–	–	–	–	–	–
LC3-TR-SHCC	29.3	22.33	29.23	1.49	0.99	40.70	0.51	−0.2

Indeed, only minimal fluctuations of the plastic deformation are expected once a certain impact velocity is exceeded. This assumption is reasonable for thin plates, but requires further experimental validation as it has not been extensively investigated in the literature.

Nevertheless, following this phenomenological approach, important mechanical parameters can be estimated and compared, such as the elastic limit of the composite (v_{el}), the maximum inelastic deformation as the relative maximum within the transition domain ($u_{res,max}$), and the stabilisation conditions (v_{stab}, u_{stab}), after which the inelastic deflection is only slightly affected by increasing input velocity extents. All these values, estimated according to the previous assumptions, are reported in Table 5.

On the one hand, in the rebound domain, the response of the specimen features a quasi-elastic character, associated with nearly total or partial recovery of the deflection, resulting in little inelastic deformation of the plate. On the other hand, in the far perforation domain, a brittle and localised response again leads to a less pronounced pseudo-plastic behaviour. Focusing instead on the transition region, the maximisation of the fitting curve yields values very close to the ballistic limit calculated by the bilinear approach previously discussed, deviating by about 12% in case of Ref-TRC [26] and between 0.2% and 2.8% in the case of the composite systems scrutinised here. This finding confirms what was envisaged by analysing the deflection maps in Figs. 15 and 17 for penetration (inlets *a*) and far perforation (inlets *b*) cases. According to this evidence, the penetration limit condition is correlated with the highest inelastic deflection magnitude. This is in line with the observations discussed by Wastiels et al. [32].

When assessing the peak residual deflection ($u_{res,max}$), the highest and the lowest values among the available data sets are exhibited by the Ref-TRC and hybrid composite plates, respectively. This emphasises the key role played by the dispersed fibres in mitigating the permanent deflection of the plates. Furthermore, u_{stab} for LC3-SHCC is about 11% lower than its FA-SHCC counterpart. This can be attributed to the different mechanical properties of the two binders, and in particular, to the slightly higher elastic limit (v_{el}) of the LC^3 binder.

3.2.4. Impact safety outlook

The abrupt spalling of concrete fragments upon a collision is a serious threat to human safety and can jeopardise the integrity of structures and goods. Confinement and debris retention by mineral-bonded composites as a strengthening layer during extreme events represent a design consideration of paramount importance. Fig. 20a plots the total mass of ejected fragments, normalised to the initial mass of the plate, after collision at varying striking velocities, v_1. A smooth linear trend is observed, whose linear fit features robust coefficients of determination (R^2) ranging between 0.86 and 0.92.

It is noteworthy that the presence of the two-layer textile reinforcement alone is not sufficient to prevent spalling, as it is not able to contrast the abrupt fragmentation of the brittle matrix, confirming the observations made in Section 3.2.1 on failure modes. Indeed, the Ref-TRC plate tested in the rebound domain, despite the limited impact energy, still records some concrete spalling, about 1.5% of the initial mass, as a consequence of the crushing of the concrete in the impacted face.

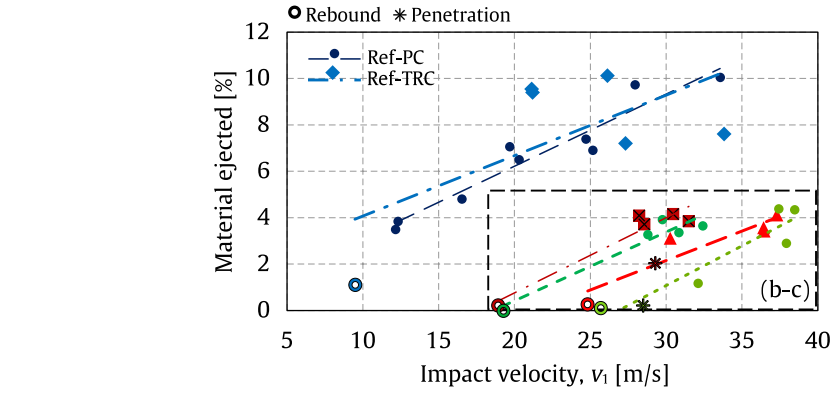

(a) Comparison with reference plates

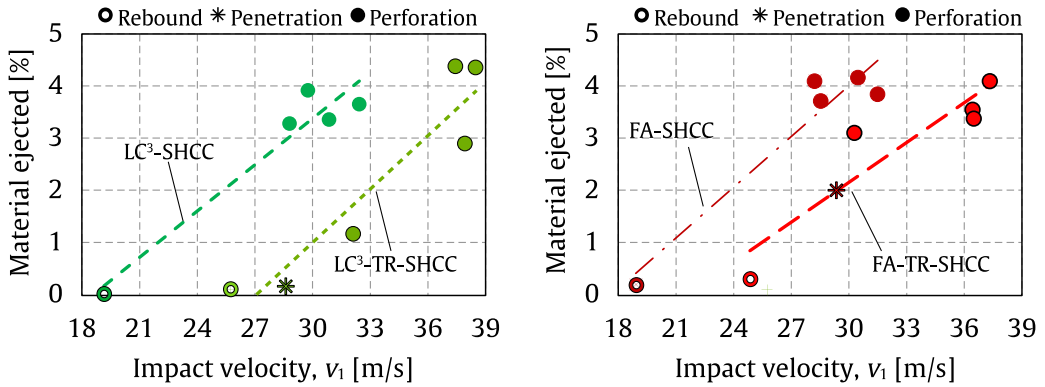

(b) LC^3 (c) FA

Fig. 20. Linearly increasing trends of the mass of fragments ejected from the plates (normalised to the initial mass of the plate) as a function of the input velocity v_1.

The addition of short dispersed fibres results in improved matrix integrity, associated with a significant reduction in the number of fragments ejected from the plate [67]. Indeed, no expelled debris is observed in the rebound case for SHCC and TR-SHCC plates, owing to the efficient stitching action of the fibres. The additional contribution of textiles to matrix retention is clearly visible in the zoomed inlets in Fig. 20b and c, with consistently lower spalling observed as compared to the corresponding SHCC samples. The effect of the binder can also be pinpointed. The use of LC^3 blended binder entails the system with a slightly higher retention capability upon collision when compared to the FA counterpart. The bar charts in Fig. 21 compare the ejected mass at the fixed impact velocity of 28 m/s, which is the highest common value for all groups tested.

At this moderate impact velocity level, the TR-SHCC specimens are close to their penetration limit, while all other samples are fully perforated. The LC3-SHCC composite scores a 50% reduction in debris spalling compared to its Ref-TRC counterpart, while a reduction of about 95% is achieved when the hybrid reinforcement is considered. This result emphasises that textile reinforced composites in impact protection represent a very attractive solution to increase the safety of the built environment, as long as the embedding matrix possesses a certain degree of ductility to retain debris spalling. A consistent benefit of the LC^3-based composites is demonstrated for both SHCC and hybrid configurations, resulting in a spalling reduction of approximately 20% for corresponding SHCC plates and as much as 60% for hybrid ones including the FA blended binder.

4. Summary and conclusions

In this study, the characterisation of four different mineral-bonded high performance composite materials under impact loading was experimentally assessed. The tests were performed on thin plates taking advantage of an air-pressure drop-tower facility. The composites under investigation are intended as thin reinforcing layers to be applied to concrete substrates of aged or damaged members to entail them with additional ductility resources and damage tolerance. To this end, the addition of short synthetic microfibres and high-strength carbon textiles was investigated to appraise their synergistic interaction. A novel inorganic matrix made of LC^3 binder was characterised and compared with a reference mix containing fly ash as a supplementary cementitious

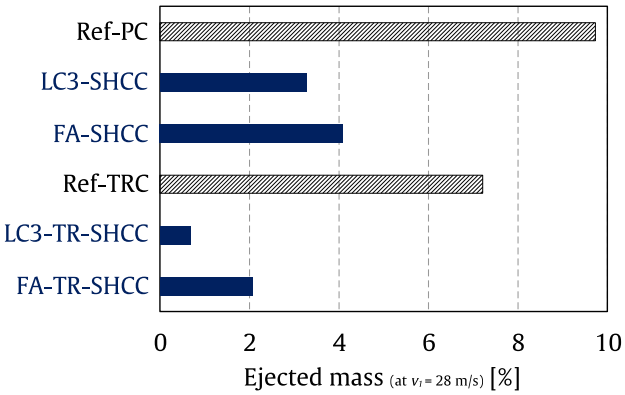

Fig. 21. Debris mass at the fixed impact velocity of (28 ± 2) m/s.

material, at the same extent of cement replacement. Both matrices were designed for advanced application techniques, such as shotcrete and extrusion. Several impact velocity levels were considered to determine the ballistic limit of the different composites, i.e. the minimum impact energy required to perforate the plate, as well as to assess the damage with respect to impact safety. Comparing the experimental results obtained in the current investigation with previous tests on plain fine-grained concrete and textile-reinforced concrete (TRC), the following conclusions can be drawn:

- Concrete used for structural strengthening is an inherently brittle material. This lack of ductility can be mitigated by the addition of textiles, however, textiles alone are unable to prevent matrix spalling.
- In TRC specimens, matrix brittleness results in a high concentration of damage in the proximity of the projectile imprint, associated with severe shear acting on the textile.
- The addition of ductile short fibres significantly improves the damage tolerance of reinforcing materials, entailing the brittle matrix with a quasi-ductile behaviour due to wider and uniform damage propagation and crack branching.
- The stitching and crack-bridging actions of the fibres foster the impact safety of mineral-bonded composites by minimising the amount of material ejected from the specimen upon collision.
- The synergistic interaction between fibres and textiles is responsible for a noteworthy increase in the ballistic limit of the composite plates, which cannot be achieved by using alternatively short fibres or textile meshes alone. This is ascribed to the effective propagation of damage induced by short fibres, which activate a wider portion of the textiles, which act as a membrane.
- Experimental evidence envisions a close relationship between the inelastic deflection in the vicinity of the impact crater and the ballistic limit.

While a variety of strengthening measures can certainly improve the impact response of concrete members, the particular advantage of SHCC and hybrid reinforcing solutions lies in the very limited amount of additional structural mass through thin and highly optimised composite elements. At the same time, a significant increase in impact safety is attained, resulting in a sustainable and resource-efficient strengthening method.

CRediT authorship contribution statement

Cesare Signorini: Conceptualization, Methodology, Validation, Data curation, Writing – original draft, Writing – review & editing, Visualisation, Supervision, Project administration. **Franz Bracklow:** Formal analysis, Validation, Investigation, Data curation, Visualisation, Writing – review & editing. **Marcus Hering:** Conceptualization, Methodology, Supervision. **Marko Butler:** Conceptualization, Resources, Writing – review & editing, Supervision. **Lena Leicht:** Investigation. **Thomas Schubert:** Investigation. **Mirza A.B. Beigh:** Investigation. **Birgit Beckmann:** Resources, Writing – review & editing, Supervision. **Manfred Curbach:** Resources, Supervision, Funding acquisition. **Viktor Mechtcherine:** Conceptualisation, Resources, Writing – review & editing, Supervision, Funding acquisition.

Declaration of competing interest

The authors declare that they have no known competing financial interests or personal relationships that could have appeared to influence the work reported in this paper.

Data availability

Data will be made available on request.

Funding

The financial support of the German Research Foundation (Deutsche Forschungsgemeinschaft, DFG) in the framework of the Research Training Group (Graduiertenkollegs, GRK) 2250, entitled "*Mineral-bonded composites for enhanced structural impact safety*" (grant nr. 287321140) is gratefully acknowledged. All authors approved the final version of manuscript to be published.

References

[1] B. Beckmann, A. Hummeltenberg, T. Weber, M. Curbach, Concrete under high strain rates: Local material and global structure response to impact loading, Int. J. Protective Struct. 2 (3) (2011) 283–293.
[2] A. Hummeltenberg, B. Beckmann, T. Weber, M. Curbach, Investigation of concrete slabs under impact load, Appl. Mech. Mater. 82 (2011) 398–403.
[3] M.K. Askar, A.F. Hassan, Y.S. Al-Kamaki, Flexural and shear strengthening of reinforced concrete beams using FRP composites: A state of the art, Case Stud. Constr. Mater. (2022) e01189.
[4] Q. Jin, V.C. Li, Structural and durability assessment of ECC/concrete dual-layer system for tall wind turbine towers, Eng. Struct. 196 (2019) 109338.
[5] E. Jacques, A. Lloyd, P. Imbeau, D. Palermo, J. Quek, GFRP-retrofitted reinforced concrete columns subjected to simulated blast loading, J. Struct. Eng. 141 (11) (2015) 04015028.
[6] C.M. Jackson, E. Jacques, M. Saatcioglu, Blast retrofit of one-way reinforced concrete members using externally bonded FRP and FRP anchorage, Int. J. Protective Struct. 13 (2) (2022) 209–235.
[7] T.M. Pham, H. Hao, Review of concrete structures strengthened with FRP against impact loading, Structures 7 (2016) 59–70.
[8] C. Signorini, V. Mechtcherine, Strain-hardening cement-based composites (SHCC) for impact strengthening of buildings: Recent advances in the DFG research training group 2250, in: M. Kunieda, T. Kanakubo, T. Kanda, K.e. Kobayashi (Eds.), Strain Hardening Cementitious Composites: SHCC5, in: RILEM Bookseries, vol. 39, Springer, 2023, pp. 281–290.
[9] T. Trapko, The effect of high temperature on the performance of CFRP and FRCM confined concrete elements, Composites B 54 (2013) 138–145.
[10] M. Messori, A. Nobili, C. Signorini, A. Sola, Effect of high temperature exposure on epoxy-coated glass textile reinforced mortar (GTRM) composites, Constr. Build Mater. 212 (2019) 765–774.
[11] J. Donnini, F.D.C. y Basalo, V. Corinaldesi, G. Lancioni, A. Nanni, Fabric-reinforced cementitious matrix behavior at high-temperature: Experimental and numerical results, Composites B 108 (2017) 108–121.
[12] A.B. Elnagar, H.M. Afefy, A.T. Baraghith, M.H. Mahmoud, Experimental and numerical investigations on the impact resistance of SHCC-strengthened RC slabs subjected to drop weight loading, Constr. Build. Mater. 229 (2019) 116866.
[13] T.C.S. Figueiredo, C.M. Gaspar, M. Hering, I. Curosu, M. Curbach, V. Mechtcherine, F. de Andrade Silva, Experimental modal analysis of RC beams strengthened with SHCC subjected to shear under impact strain rates, Eng. Struct. 264 (2022) 114459.
[14] V.C. Li, On engineered cementitious composites (ECC) a review of the material and its applications, J. Adv. Concr. Technol. 1 (3) (2003) 215–230.
[15] C. Signorini, A. Sola, B. Malchiodi, A. Nobili, Highly dissipative fiber-reinforced concrete for structural screeds, J. Mater. Civ. Eng. 34 (4) (2022) 04022022.
[16] Q. Jin, V.C. Li, Development of lightweight engineered cementitious composite for durability enhancement of tall concrete wind towers, Cem. Concr. Compos. 96 (2019) 87–94.
[17] V. Mechtcherine, O. Millon, M. Butler, K. Thoma, Mechanical behaviour of strain hardening cement-based composites under impact loading, Cem. Concr. Compos. 33 (1) (2011) 1–11.
[18] A.A. Heravi, I. Curosu, V. Mechtcherine, A gravity-driven split Hopkinson tension bar for investigating quasi-ductile and strain-hardening cement-based composites under tensile impact loading, Cem. Concr. Compos. 105 (2020) 103430.
[19] E. Cadoni, D. Forni, E. Bonnet, S. Dobrusky, Experimental study on direct tensile behaviour of UHPFRC under high strain-rates, Constr. Build. Mater. 218 (2019) 667–680.
[20] A. Tawfik, I. Curosu, G. Alsous, V. Mechtcherine, A testing device to investigate the properties of strain-hardening, cement-based composites (SHCC) under impact shear loading, Int. J. Impact Eng. 167 (2022) 104280.
[21] A. Tawfik, C. Signorini, V. Mechtcherine, Direct assessment of the shear behavior of strain-hardening cement-based composites under quasi-static and impact loading: Influence of shear span and notch depth, Cem. Concr. Compos. 140 (2023) 105119.
[22] R. Yu, L. Van Beers, P. Spiesz, H. Brouwers, Impact resistance of a sustainable ultra-high performance fibre reinforced concrete (UHPFRC) under pendulum impact loadings, Constr. Build. Mater. 107 (2016) 203–215.
[23] J. Zhang, M. Maalej, S.T. Quek, Performance of hybrid-fiber ECC blast/shelter panels subjected to drop weight impact, J. Mater. Civ. Eng. 19 (10) (2007) 855–863.
[24] Y. Liu, Y. Wei, Drop-weight impact resistance of ultrahigh-performance concrete and the corresponding statistical analysis, J. Mater. Civ. Eng. 34 (1) (2022) 04021409.
[25] E. Tamsen, I. Curosu, V. Mechtcherine, D. Balzani, Computational micro-macro analysis of impact on strain-hardening cementitious composites (SHCC) including microscopic inertia, Materials 13 (21) (2020) 4934.
[26] M. Hering, T. Kühn, M. Curbach, Small-scale plate tests with fine concrete in experiment and first simplified simulation, Struct. Concr. 22 (2) (2021) 637–649.
[27] B. Batarlar, M. Hering, F. Bracklow, T. Kühn, B. Beckmann, M. Curbach, Experimental investigation on reinforced concrete slabs strengthened with carbon textiles under repeated impact loads, Struct. Concr. 22 (1) (2021) 120–131.
[28] M. Hering, M. Curbach, Strengthening of RC plates with mineral-bonded composite layers for enhanced impact safety, in: MATEC Web of Conferences, Vol. 323, EDP Sciences, 2020, p. 01015.
[29] V. Mechtcherine, Novel cement-based composites for the strengthening and repair of concrete structures, Constr. Build. Mater. 41 (2013) 365–373.
[30] T. Gong, I. Curosu, F. Liebold, D.M. Vo, K. Zierold, H.-G. Maas, C. Cherif, V. Mechtcherine, Tensile behavior of high-strength, strain-hardening cement-based composites (HS-SHCC) reinforced with continuous textile made of ultra-high-molecular-weight polyethylene, Materials 13 (24) (2020) 5628.
[31] D. Liu, B.B. Raju, X. Dang, Impact perforation resistance of laminated and assembled composite plates, Int. J. Impact Eng. 24 (6–7) (2000) 733–746.
[32] J. Wastiels, J. Van Ackeren, T. Tysmans, W. Van Paepegem, Flexural impact response of textile reinforced inorganic phosphate cement composites (TRC), Constr. Build. Mater. 163 (2018) 296–304.
[33] F. Bracklow, M. Hering, B. Beckmann, M. Curbach, Impact experiments on differently reinforced concrete plates, in: SMiRT26: 26th International Conference on Structural Mechanics in Reactor Technology, IASMiRT, 2022.
[34] F. Vossoughi, C.P. Ostertag, P.J. Monteiro, G.C. Johnson, Resistance of concrete protected by fabric to projectile impact, Cem. Concr. Res. 37 (1) (2007) 96–106.
[35] Y. Peng, H. Wu, Q. Fang, Z. Gong, X. Kong, A note on the deep penetration and perforation of hard projectiles into thick targets, Int. J. Impact Eng. 85 (2015) 37–44.
[36] A. Rajput, M.A. Iqbal, N. Gupta, Ballistic performances of concrete targets subjected to long projectile impact, Thin-Walled Struct. 126 (2018) 171–181.

[37] B. Tahenti, F. Coghe, R. Nasri, Ballistic limit estimation approaches for ballistic resistance assessment, Def. Sci. J. 70 (1) (2020) 82–89, http://dx.doi.org/10.14429/dsj.70.14122.
[38] L. Jinzhu, L. Zhongjie, Z. Hongsong, H. Fenglei, Perforation experiments of concrete targets with residual velocity measurements, Int. J. Impact Eng. 57 (2013) 1–6.
[39] A.N. Dancygier, Effect of reinforcement ratio on the resistance of reinforced concrete to hard projectile impact, Nucl. Eng. Des. 172 (1–2) (1997) 233–245.
[40] X. Chen, X. Li, F. Huang, H. Wu, Y. Chen, Normal perforation of reinforced concrete target by rigid projectile, Int. J. Impact Eng. 35 (10) (2008) 1119–1129.
[41] Y. Peng, H. Wu, Q. Fang, J. Liu, Z. Gong, Residual velocities of projectiles after normally perforating the thin ultra-high performance steel fiber reinforced concrete slabs, Int. J. Impact Eng. 97 (2016) 1–9.
[42] M. Hering, J. Sievers, M. Curbach, B. Beckmann, An approach to predicting the ballistic limit of thin textile-reinforced concrete plates based on experimental results, Buildings 13 (9) (2023) 2234.
[43] K. Scrivener, A. Favier, et al., Calcined Clays for Sustainable Concrete, Springer, 2015.
[44] M.A. Yazdi, M. Liebscher, S. Hempel, J. Yang, V. Mechtcherine, Correlation of microstructural and mechanical properties of geopolymers produced from fly ash and slag at room temperature, Constr. Build. Mater. 191 (2018) 330–341.
[45] L. Wang, Z. Zhu, A.H. Ahmed, M. Liebscher, X. Zhu, V. Mechtcherine, Self-healing behavior of high-strength strain-hardening cement-based composites (HS-SHCC) blended with limestone calcined clay cement (LC^3), Constr. Build. Mater. 370 (2023) 130633.
[46] F. Avet, R. Snellings, A.A. Diaz, M.B. Haha, K. Scrivener, Development of a new rapid, relevant and reliable (R3) test method to evaluate the pozzolanic reactivity of calcined kaolinitic clays, Cem. Concr. Res. 85 (2016) 1–11.
[47] L. Wang, N.U. Rehman, I. Curosu, Z. Zhu, M.A.B. Beigh, M. Liebscher, L. Chen, D.C. Tsang, S. Hempel, V. Mechtcherine, On the use of limestone calcined clay cement (LC^3) in high-strength strain-hardening cement-based composites (HS-SHCC), Cem. Concr. Res. 144 (2021) 106421.
[48] A.H. Ahmed, S. Nune, M. Liebscher, T. Köberle, A. Willomitzer, I. Noack, M. Butler, V. Mechtcherine, Exploring the role of dilutive effects on microstructural development and hydration kinetics of limestone calcined clay cement (LC^3) made of low-grade raw materials, J. Cleaner Product. (2023) 139438, http://dx.doi.org/10.1016/j.jclepro.2023.139438.
[49] T. Gong, A.A. Heravi, G. Alsous, I. Curosu, V. Mechtcherine, The impact-tensile behavior of cementitious composites reinforced with carbon textile and short polymer fibers, Appl. Sci. 9 (19) (2019) 4048.
[50] EuroFibers BV, Dyneema® UHMWPE fiber: Product overview, 2019, https://eurofibers.com/wp-content/uploads/2019/05/WEB-DYNEEMA_Leaflet_2019-04.pdf. (Accessed 04 October 2023).
[51] T. Gong, A.H. Ahmed, I. Curosu, V. Mechtcherine, Tensile behavior of hybrid fiber reinforced composites made of strain-hardening cement-based composites (SHCC) and carbon textile, Constr. Build. Mater. 262 (2020) 120913.
[52] I. Curosu, M. Liebscher, G. Alsous, E. Muja, H. Li, A. Drechsler, R. Frenzel, A. Synytska, V. Mechtcherine, Tailoring the crack-bridging behavior of strain-hardening cement-based composites (SHCC) by chemical surface modification of poly (vinyl alcohol)(PVA) fibers, Cem. Concr. Compos. 114 (2020) 103722.
[53] M. Hering, Investigation of Mineral-Bonded Strengthening Layers for Reinforced Concrete Plates Against Impact Loads, Technische Universität Dresden, Dresden, 2020, http://dx.doi.org/10.2314/GBV:868615218.
[54] I. Curosu, M. Liebscher, V. Mechtcherine, C. Bellmann, S. Michel, Tensile behavior of high-strength strain-hardening cement-based composites (HS-SHCC) made with high-performance polyethylene, aramid and PBO fibers, Cem. Concr. Res. 98 (2017) 71–81.
[55] A.C.C. Trindade, A.A. Heravi, I. Curosu, M. Liebscher, F. de Andrade Silva, V. Mechtcherine, Tensile behavior of strain-hardening geopolymer composites (SHGC) under impact loading, Cem. Concr. Compos. 113 (2020) 103703.
[56] I. Curosu, V. Mechtcherine, D. Forni, E. Cadoni, Performance of various strain-hardening cement-based composites (SHCC) subject to uniaxial impact tensile loading, Cem. Concr. Res. 102 (2017) 16–28.
[57] S. Gopinath, A. Prakash, A.F. Ahmed, Synergy of hybrid textile reinforced concrete under impact loading, Sādhanā 45 (2020) 1–11.
[58] P. Máca, R. Sovják, P. Konvalinka, Mix design of UHPFRC and its response to projectile impact, Int. J. Impact Eng. 63 (2014) 158–163.
[59] S. Liu, D. Zhu, G. Li, Y. Yao, Y. Ou, C. Shi, Y. Du, Flexural response of basalt textile reinforced concrete with pre-tension and short fibers under low-velocity impact loads, Constr. Build. Mater. 169 (2018) 859–876.
[60] M. Tsesarsky, A. Peled, A. Katz, I. Anteby, Strengthening concrete elements by confinement within textile reinforced concrete (TRC) shells–Static and impact properties, Constr. Build. Mater. 44 (2013) 514–523.
[61] S. Liu, D. Zhu, X. Wang, C. Shi, Pullout properties of AR-glass textile embedded in cement matrix under different velocities and temperatures, Constr. Build. Mater. 228 (2019) 116779.
[62] D. Schmitt, T. Kühn, O. Millon, A. Stolz, S. Nau, M. Curbach, K. Thoma, Strukturdynamisches Verhalten von Stahlbetonplatten unter Impakteinwirkung bei variablen Geschwindigkeiten, Beton-und Stahlbetonbau 114 (8) (2019) 526–536.
[63] H. Grisaro, A.N. Dancygier, A modified energy method to assess the residual velocity of non-deforming projectiles that perforate concrete barriers, Int. J. Protective Struct. 5 (3) (2014) 307–321.
[64] M. Maalej, S.T. Quek, J. Zhang, Behavior of hybrid-fiber engineered cementitious composites subjected to dynamic tensile loading and projectile impact, J. Mater. Civ. Eng. 17 (2) (2005) 143–152.
[65] G. Corbett, S. Reid, W. Johnson, Impact loading of plates and shells by free-flying projectiles: a review, Int. J. Impact Eng. 18 (2) (1996) 141–230.
[66] D.-Y. Yoo, N. Banthia, S.-W. Kim, Y.-S. Yoon, Response of ultra-high-performance fiber-reinforced concrete beams with continuous steel reinforcement subjected to low-velocity impact loading, Compos. Struct. 126 (2015) 233–245.
[67] R. Sovjak, T. Vavřiník, J. Zatloukal, P. Maca, T. Mičunek, M. Frydrỳn, Resistance of slim UHPFRC targets to projectile impact using in-service bullets, Int. J. Impact Eng. 76 (2015) 166–177.